

Non-oscillatory entropy stable DG schemes for hyperbolic conservation law

Yuchang Liu¹, Wei Guo², Yan Jiang³, and Mengping Zhang⁴

Abstract: In this paper, we propose a class of non-oscillatory, entropy-stable discontinuous Galerkin (NOES-DG) schemes for solving hyperbolic conservation laws. By incorporating a specific form of artificial viscosity, our new scheme directly controls entropy production and suppresses spurious oscillations. To address the stiffness introduced by the artificial terms, which can restrict severely time step sizes, we employ the integration factor strong stability-preserving Runge-Kutta method for time discretization. Furthermore, our method remains compatible with positivity-preserving limiters under suitable CFL conditions in extreme cases. Various numerical examples demonstrate the efficiency of the proposed scheme, showing that it maintains high-order accuracy in smooth regions and avoids spurious oscillations near discontinuities.

Key Words: hyperbolic conservation laws, discontinuous Galerkin method, entropy stability, nonoscillatory.

1 Introduction

In this paper, we focus on simulating hyperbolic conservation laws, which describe how the balance of conserved quantities within a domain is determined by the flux across its boundaries. A celebrated example is the compressible Euler equations in gas dynamics. The discontinuous Galerkin (DG) method has emerged as a powerful and versatile tool for solving these problems, offering several distinctive advantages such as local conservation, high order accuracy, flexibility in handling complex geometries and general boundary conditions, as well as ease of adaptivity and parallel implementation. However, challenges remain in approximating the entropy solution with both numerical and theoretical justifications. The entropy solution is the unique physically relevant weak solution characterized by fulfilling entropy inequalities. Numerical methods that preserve

¹School of Mathematical Sciences, University of Science and Technology of China, Hefei, Anhui 230026, P.R. China. E-mail: lissandra@mail.ustc.edu.cn.

²Department of Mathematics and Statistics, Texas Tech University, Lubbock, TX, 79409, USA. E-mail: weimath.guo@ttu.edu. Research supported by NSF grant NSF-DMS-2111383, Air Force Office of Scientific Research FA9550-18-1-0257.

³School of Mathematical Sciences, University of Science and Technology of China, Hefei, Anhui 230026, P.R. China. E-mail: jiangy@ustc.edu.cn. Research supported by NSFC grant 12271499 and Cyrus Tang Foundation.

⁴School of Mathematical Sciences, University of Science and Technology of China, Hefei, Anhui 230026, P.R. China. E-mail: mpzhang@ustc.edu.cn.

these inequalities at the discrete level are called *entropy stable*. Under certain conditions, such schemes can recover the desired entropy solution upon convergence, see [27]. Meanwhile, the entropy solution may develop discontinuities or sharp gradient structures in finite time. Even entropy stable schemes may still produce spurious oscillations in the presence of such singular structures. These oscillations can severely contaminate approximation accuracy or lead to simulation failure. Therefore, novel techniques are needed to remove oscillations while preserving the entropy stability property. The main objective of this work is to develop a simple, computationally efficient, and theoretically justified DG method that can simultaneously achieve discrete entropy stability and avoid nonphysical oscillations.

The past few decades have witnessed the tremendous development of the provably entropy conservative and entropy stable numerical methods. Notably, in the seminal work by Tadmor [36, 37], the concepts of entropy conserving and entropy stable numerical fluxes were introduced in the context of finite volume schemes. This foundational work has significantly influenced the subsequent developments. For instance, in [28], a procedure was proposed for designing high-order entropy conservative fluxes. Building upon these components, an entropy stable and arbitrarily high order version of ENO schemes, termed TeCNO, was developed in [14]. Within the framework of DG discretization, it is shown in [23] that the classic semi-discrete DG scheme is entropy stable. However, this property is limited to the square entropy function and requires exact integration. To ensure entropy stability for a general entropy function and under quadrature approximations, two primary approaches have been developed. The first approach leverages the summation-by-parts (SBP) methodology [11, 12, 35, 10, 21]. Pioneering contributions include [3, 16, 17]. Furthermore, in [7], a Gauss-Lobatto quadrature-based entropy stable DG scheme is developed by introducing SBP operators in conjunction with the flux differencing technique [13, 3, 2]. In [4, 5], a set of entropy stable DG methods allowing for arbitrary quadrature rules is developed by designing the hybridized SBP operators that combine the volume and surface quadrature nodes. The second approach was first introduced in [1], which seeks to explicitly control the production of entropy within each element by incorporating an artificial term in the DG weak formulation. Unlike the first approach, it does not rely on the flux differencing technique. In [15], inspired by [1], a fully discrete entropy conservative DG method under the ADER framework is proposed by choosing a novel artificial diffusion term for entropy correction together with the relaxation approach for time integration [24]. However, this approach cannot effectively handle problems with discontinuous solutions, as it lacks the ability to control spurious oscillations.

In this work, motivated by [15], we develop a class of provably (in the semi-discrete sense) high order and entropy stable DG methods that preserve all desired properties of the classic DG method and is capable of eliminating spurious oscillations in the presence of shocks. The difficulty lies in the design of an artificial term that can simultaneously control entropy production and oscillations, as well as preserve the original high order accuracy. Furthermore, it is also desired that the modified formulation is convenient to

implement and cost-effective. To address this, we generalize the entropy-based artificial diffusion framework [18] by incorporating an idea from the essentially oscillation-free DG (OFDG) method [32]. The OFDG method employs a projection-based damping term in the DG formulation to control spurious oscillations. In particular, the damping coefficient is adaptively adjusted by measuring discontinuity intensity, decreasing in smooth regions and increasing near discontinuities. In this work, we employ an artificial diffusion term rather than a damping term, and furthermore, the coefficient is determined to ensure both the entropy stability and oscillation-free property. Our work introduces three key improvements over existing approaches. First, in [15], the authors claimed that an arbitrary piecewise polynomial approximation or interpolation with desired high order accuracy for the entropy variable can ensure the entropy dissipation property. However, we disprove this claim by providing a counterexample. Moreover, we demonstrate that a specific interpolation property is required for ensuring provable entropy stability. Second, as mentioned in [8], the denominator of the coefficient in the entropy correction term can approach zero more rapidly than the numerator, potentially compromising accuracy. To circumvent the difficulty, we propose to further incorporate the oscillation coefficient to control the main coefficient, thereby preserving the accuracy of the scheme. Last, the proposed method attempts to directly control entropy production, allowing it to accommodate arbitrary monotone numerical fluxes and quadrature rules. Moreover, the algorithm can be implemented by reusing a classic DG code with only the artificial viscosity term added, significantly reducing development time.

Note that the proposed entropy artificial viscosity term may incur additional stiffness, which can lead to stringent CFL time step restriction when a standard explicit strong-stability-preserving Runge-Kutta (SSP-RK) time discretization is used. To address this issue, we implement the explicit integral factor SSP-RK time discretization [6], which can greatly mitigate the time step constraint. Furthermore, for extreme problems such as the high Mach number astrophysical jet problem, it is necessary to ensure positivity of density and pressure to avoid simulation failures. Note that, as the artificial viscosity term is locally conservative, we can further adapt the positivity-preserving limiter developed in [41] with an appropriate adjustment on the CFL condition.

The rest of this paper is organized as follows. In Section 2, we introduce the formulation of semi-discrete non-oscillatory entropy stable DG schemes for both one-dimensional and two-dimensional scalar equations and systems, along with theoretical analysis on mass conservation, discrete entropy stability, and error estimation. In section 3, we present the fully discrete formulations, integrating an integral factor SSP-RK time discretization and a modified positivity-preserving limiter. In Section 4, various numerical examples are provided to demonstrate the efficiency and efficacy of our proposed scheme. The conclusions are discussed in Section 5.

2 Semi-discrete entropy stable DG schemes

2.1 1D scalar cases

Consider the following one-dimensional scalar conservation law

$$\begin{cases} u_t + f(u)_x = 0, & x \in \Omega = [a, b], t > 0, \\ u(x, 0) = u_0(x). \end{cases} \quad (2.1)$$

For simplicity, we assume that the exact solution has either periodic or compact support boundary conditions on domain Ω .

Let (U, F) denote an entropy pair, satisfying the relation $F'(u) = U'(u)f'(u)$. Denote the entropy variable by $v = U'(u)$, and define $A(u) = U''(u)^{-1}$ which is always non-negative. Then a weak solution of (2.1) is called an *entropy solution* if for all entropy pairs, we have that

$$U(u)_t + F(u)_x \leq 0 \quad (2.2)$$

in the weak form. Furthermore, integrating the entropy condition (2.2) in space, we get

$$\frac{d}{dt} \int_{\Omega} U(u) dx \leq 0. \quad (2.3)$$

This means that the total entropy is non-increasing with respect to time. In the following, we will design a DG scheme to satisfy the inequality (2.2) or (2.3) numerically.

2.1.1 The classical DG discretization

We start with the classical DG scheme for (2.1). Suppose the domain is divided into cells

$$a = x_{1/2} < x_{3/2} < \cdots < x_{N+1/2} = b, \quad h_i = x_{i+1/2} - x_{i-1/2}.$$

Let $K_i = [x_{i-1/2}, x_{i+1/2}]$ be the cell with its center $x_i = (x_{i+1/2} + x_{i-1/2})/2$, and $\mathcal{K} = \{K_i\}$ be the collocation of all cells. Without loss of generality, we assume the mesh is uniform and denote by $h = h_i$.

Define the finite element space as

$$V_h^k = \{w(x) : w(x)|_K \in P^k(K), \forall K \in \mathcal{K}\}, \quad (2.4)$$

where $P^k(K)$ is the space of polynomials of degree at most k on cell K . Notice that for any $w \in V_h^k$, it can be discontinuous at the cell boundary $x_{i\pm 1/2}$. In the following, we let $w_{i+1/2}^+$ (resp. $w_{i+1/2}^-$) denote the limiting value of w at $x_{i+1/2}$ from the element K_{i+1} (resp. K_i), $[w]_{i+1/2} = w_{i+1/2}^+ - w_{i+1/2}^-$ denote its jump, and $\{w\}_{i+1/2} = \frac{1}{2}(w_{i+1/2}^+ + w_{i+1/2}^-)$ be its average at $x_{i+1/2}$.

The semi-discrete DG scheme is defined as: seek $u_h \in V_h^k$, such that for all $w \in V_h^k$ and $K_i \in \mathcal{K}$,

$$\int_{K_i} \frac{\partial u_h}{\partial t} w \, dx = \int_{K_i} f(u_h) \frac{\partial w}{\partial x} \, dx - \hat{f}_{i+1/2} w_{i+1/2}^- + \hat{f}_{i-1/2} w_{i-1/2}^+. \quad (2.5)$$

Here $\hat{f}_{i+1/2} = \hat{f}(u_h|_{i+1/2}^-, u_h|_{i+1/2}^+)$ is the monotone numerical flux at $x_{i+1/2}$. In this work, we use the local Lax-Friedrichs flux

$$\hat{f}(u^-, u^+) = \frac{1}{2} [f(u^+) + f(u^-) - \alpha(u^+ - u^-)], \quad \alpha = \max_{u \in I(u^-, u^+)} |f'(u)|,$$

where $I(u^-, u^+)$ is the interval defined between u^- and u^+ .

2.1.2 The entropy stable non-oscillatory DG schemes

Considering the equation (2.1) with an additional local viscosity in cell K_i

$$u_t + f(u)_x = \sigma_i (\nu_i(x) A(u) v(u)_x)_x, \quad x \in K_i, \quad (2.6)$$

where σ_i is a local non-negative parameter, and ν_i satisfies

$$\nu_i(x_{i-1/2}) = \nu_i(x_{i+1/2}) = 0 \quad \text{and} \quad \nu_i(x) \geq 0, \quad x \in K_i. \quad (2.7)$$

In this work, we simply let

$$\nu_i(x) = 1 - X_i^2(x), \quad X_i(x) = \frac{x - x_i}{h/2}. \quad (2.8)$$

Notice that the added viscous term is similar to that introduced in [39]. However, [39] focuses solely on eliminating spurious oscillation by adding viscosity based on the smoothness of the solution u itself. In contrast, we are more concerned with controlling entropy. The added viscosity term relies on the entropy terms $A(u)$ and $v(u)$ rather than u itself, which provides additional entropy dissipation. By carefully choosing the parameter σ_i we are able to achieve numerical entropy stability while avoiding spurious oscillations.

The semi-discrete non-oscillatory entropy stable DG scheme (denoted as NOES-DG) is defined based on the modified viscous equation (2.6): find $u_h \in V_h^k$, such that for all

$w \in V_h^k$ and $K_i \in \mathcal{K}$,

$$\begin{aligned} \int_{K_i} \frac{\partial u_h}{\partial t} w \, dx &= \int_{K_i} f(u_h) \frac{\partial w}{\partial x} \, dx - \hat{f}_{i+1/2} w_{i+1/2}^- + \hat{f}_{i-1/2} w_{i-1/2}^+ \\ &\quad - \sigma_i \int_{K_i} \nu_i \frac{\partial v_h}{\partial x} A(u_h) \frac{\partial w}{\partial x} \, dx. \end{aligned} \quad (2.9)$$

Note that $\nu_i(x)$ vanishes at $x_{i\pm 1/2}$ (2.7), and hence the boundary terms resulting from integration by parts are nullified, simplifying the numerical formulation. The function $v_h \in V_h^k$ is a piecewise polynomial approximating the entropy variable $v(u_h)$ with condition

$$v_h(x_{i+1/2}^-) = v(u_h(x_{i+1/2}^-)), \quad v_h(x_{i-1/2}^+) = v(u_h(x_{i-1/2}^+)). \quad (2.10)$$

This condition is critical for entropy control, which will be discussed in detail below. We let v_h be the $(k+1)$ -th order interpolating polynomial of $v(u_h)$ based on the Gauss-Lobatto quadrature points in K_i , hence automatically satisfying (2.10).

In addition, the parameter σ_i is defined as

$$\sigma_i = \max \{ \sigma_i^{jump}, \sigma_i^{entropy} \}, \quad (2.11)$$

where

$$\sigma_i^{jump} = c_f \left(h \| [u_h] \|_{\partial K_i} + \sum_{l=1}^k l(l+1) h^{l+1} \| [\partial_x^l u_h] \|_{\partial K_i} \right), \quad (2.12a)$$

$$\sigma_i^{entropy} = \max \left\{ \frac{F_i}{E_i}, 0 \right\}, \quad (2.12b)$$

$$E_i = \int_{K_i} \nu_i \frac{\partial v_h}{\partial x} A \frac{\partial v_h}{\partial x} \, dx, \quad (2.12c)$$

$$F_i = \hat{F}_{i+1/2} - \hat{F}_{i-1/2} - \hat{f}_{i+1/2}^C v_{i+1/2}^- + \hat{f}_{i-1/2}^C v_{i-1/2}^+ + \int_{K_i} f(u_h) \frac{\partial v_h}{\partial x} \, dx. \quad (2.12d)$$

Moreover, to ensure entropy stability, we need that the quadrature rules used to approximate the integrals in (2.9) are identical for approximating the integrals in E_i and F_i . The choice of $\sigma_i^{entropy}$ is proposed in [15] to balance the entropy production. Here, \hat{F} in (2.12d) denotes a numerical entropy flux consistent with F , i.e., $\hat{F}(u, u) = F(u)$. In this work, we choose \hat{F} to be the central flux

$$\hat{F}(u^-, u^+) = \frac{1}{2} (F(u^+) + F(u^-)). \quad (2.13)$$

Assume that the numerical flux is split into $\hat{f} = \hat{f}^C + \hat{f}^D$, where \hat{f}^C and \hat{f}^D denote the central part and the diffusive part, respectively. For example, for the Lax-Friedrichs

flux, we have

$$\hat{f}^C(u^-, u^+) = \frac{1}{2}(f(u^+) + f(u^-)), \quad \hat{f}^D(u^-, u^+) = -\frac{1}{2}\alpha(u^+ - u^-). \quad (2.14)$$

Note that several other popular monotone numerical fluxes, such as the Engquist–Osher flux and Godunov flux, allow for such a splitting [29]. Below, we will show that when $\sigma_i \geq \sigma_i^{entropy}$, the scheme is entropy stable.

Meanwhile, the DG formulation (2.9) with $\sigma_i = \sigma_i^{entropy}$, while entropy stable, may still generate spurious oscillations in the presence of strong shocks. To remedy such a drawback, we further incorporate σ_i^{jump} to suppress oscillations and let $\sigma_i = \max\{\sigma_i^{jump}, \sigma_i^{entropy}\}$. The σ_i^{jump} , originally proposed by the OFDG method [32] and slightly modified in [39], measures discontinuity intensity and is defined with

$$\|[\partial_x^l u_h]\|_{\partial K_i} = \left| \left[\frac{\partial^l u_h}{\partial x^l} \right]_{x_{i-1/2}} \right| + \left| \left[\frac{\partial^l u_h}{\partial x^l} \right]_{x_{i+1/2}} \right|.$$

Note that σ_i^{jump} is small in smooth regions, and becomes large near discontinuities.

Moreover, E_i may approach zero, causing the parameter $\sigma_i^{entropy}$ in (2.12b) to become very large. This can greatly compromise the accuracy of the scheme [8] and incur significant stiffness. Note that even for smooth problems, we do not have control over the parameter $\sigma_i^{entropy}$. As an example, consider the linear flux $f(u) = u$ with the square entropy $U(u) = u^2$, and u_h is a $(k+1)$ -th order approximate of u , then we have the estimates of F_i and E_i

$$F_i = \frac{1}{4} \left[(u_h|_{i+1/2}^+ - u_h|_{i+1/2}^-)^2 - (u_h|_{i-1/2}^+ - u_h|_{i-1/2}^-)^2 \right] \lesssim h^{2k+2}, \quad E_i \lesssim h^2.$$

Here, $A \lesssim B$ means that there exists a constant $c_0 > 0$ independent of h such that $A \leq c_0 B$. However, we cannot directly estimate the ratio F_i/E_i unless there is a strictly positive lower bound of E_i , which is not the case in practice. Therefore, in the simulation, we set

$$\sigma_i^{entropy} = \min \left\{ \max \left\{ \frac{F_i}{E_i}, 0 \right\}, C \sigma_i^{jump} \right\}, \quad (2.15)$$

instead of (2.12b) to overcome the difficulty, where $C > 1$ is a free parameter.

2.1.3 Theoretical properties

In this section, we analyze the proposed NOES-DG scheme (2.9) and establish its several theoretical properties, including mass conservation, discrete entropy stability, and error estimates.

Theorem 2.1. (Mass Conservation) *The NOES-DG scheme (2.9) is conservative,*

i.e.

$$\frac{d}{dt} \int_{\Omega} u_h dx = 0. \quad (2.16)$$

Proof. Taking $w = 1$ in (2.9), we get

$$\int_{K_i} \frac{\partial u_h}{\partial t} dx + \hat{f}_{i+1/2} - \hat{f}_{i-1/2} = 0.$$

Summing over i yields the conservation (2.16). \square

Theorem 2.2. (*Entropy stability*) *If*

$$\sigma_i^{entropy} < C \sigma_i^{jump}, \quad \forall K_i \in \mathcal{K}, \quad (2.17)$$

then the NOES-DG scheme (2.9) is entropy stable in the sense of

$$\int_{\Omega} \frac{\partial u_h}{\partial t} v_h dx \leq 0. \quad (2.18)$$

Proof. Taking $w = v_h$ in scheme (2.9), we get

$$\int_{K_i} \frac{\partial u_h}{\partial t} v_h dx \leq -\hat{F}_{i+1/2} + \hat{F}_{i-1/2} - \hat{f}_{i+1/2}^D v_h|_{i+1/2}^- + \hat{f}_{i-1/2}^D v_h|_{i-1/2}^+.$$

Sum it over i and we can obtain

$$\int_{\Omega} \frac{\partial u_h}{\partial t} v_h dx \leq - \sum_i \left(\hat{f}_{i+1/2}^D v_h|_{i+1/2}^- - \hat{f}_{i-1/2}^D v_h|_{i-1/2}^+ \right). \quad (2.19)$$

Taking advantage of the periodic or compact support boundary, we get

$$\begin{aligned} \text{RHS} &= - \sum_i \left(\hat{f}_{i+1/2}^D v_h|_{i+1/2}^- - \hat{f}_{i+1/2}^D v_h|_{i+1/2}^+ \right) \\ &= - \sum_i \frac{1}{2} \alpha_{i+1/2} \left(u_h|_{i+1/2}^+ - u_h|_{i+1/2}^- \right) \left(v_h|_{i+1/2}^+ - v_h|_{i+1/2}^- \right) \\ &= - \sum_i \frac{1}{2} \alpha_{i+1/2} \left(u_h|_{i+1/2}^+ - u_h|_{i+1/2}^- \right) \left(v \left(u_h|_{i+1/2}^+ \right) - v \left(u_h|_{i+1/2}^- \right) \right) \\ &= - \sum_i \frac{1}{2} \alpha_{i+1/2} \left(u_h|_{i+1/2}^+ - u_h|_{i+1/2}^- \right)^2 \frac{v \left(u_h|_{i+1/2}^+ \right) - v \left(u_h|_{i+1/2}^- \right)}{u_h|_{i+1/2}^+ - u_h|_{i+1/2}^-} \\ &= - \sum_i \frac{1}{2} \alpha_{i+1/2} \left(u_h|_{i+1/2}^+ - u_h|_{i+1/2}^- \right)^2 U''(\xi) \leq 0, \end{aligned} \quad (2.20)$$

where $\xi \in I(u_h|_{i+1/2}^-, u_h|_{i+1/2}^+)$. Then, we can have (2.18). \square

Remark 2.1. In this proof, we observe the necessity of v_h to satisfy the equation (2.10), as we must have $v(u_h|_{i\pm 1/2}^\mp) = v_h|_{i\pm 1/2}^\mp$ in the third equation of (2.20). In [15], the authors claimed that $v_h \in V_h^k$ can be an arbitrary piecewise polynomial approximation of $v(u_h)$, because they believed that the following inequality always holds

$$-\sum_i \left(\hat{f}_{i+1/2}^D v_h|_{i+1/2}^- - \hat{f}_{i-1/2}^D v_h|_{i-1/2}^+ \right) \leq 0. \quad (2.21)$$

Thus, (2.19) directly leads to (2.18). However, we have found that (2.21) is not always valid, as demonstrated by the following counterexample. Assume $\Omega = [-1, 2]$ is divided by a single element $K = \Omega$, and consider the entropy function $U(u) = -\ln u$. The numerical solution is a P^2 polynomial $u_h(x) = x^2 + 1$, extended periodically. Consequently, we have $v(u_h) = -1/(x^2 + 1)$. If we define v_h as the interpolation of $v(u_h)$ at $x = -1^+$, $x = -0.9$ and $x = -0.8$, then we obtain that $v_h|_{1/2}^- = v_h(2^-) < v_h(-1^+) = v_h|_{-1/2}^+ = v_h|_{1/2}^+$. Moreover, it is obvious that $u_h|_{1/2}^- = u_h(2^-) > u_h(-1^+) = u_h|_{-1/2}^+ = u_h|_{1/2}^+$. Now we have

$$-\left(\hat{f}_{1/2}^D v_h|_{1/2}^- - \hat{f}_{-1/2}^D v_h|_{-1/2}^+ \right) = -\alpha_{1/2} \left(u_h|_{1/2}^+ - u_h|_{1/2}^- \right) \left(v_h|_{1/2}^+ - v_h|_{1/2}^- \right) > 0,$$

which contradicts (2.21). This indicates that v_h cannot be chosen as an arbitrary piecewise polynomial approximation or interpolation of $v(u_h)$. However, with the condition (2.10), we are able to show that (2.21) holds.

Remark 2.2. Although $u_x = Av_x$ holds for the exact solution, we must use the form $A(u_h) \frac{\partial v_h}{\partial x}$ in the last term of (2.9) instead of $\frac{\partial u_h}{\partial x}$. This guarantees that, when taking $w = v_h$ in (2.9), the integral in the last term could be non-negative, allowing us to finally arrive at (2.18).

Remark 2.3. For the general entropy functions, we have that

$$\begin{aligned} \int_{\Omega} \frac{\partial u_h}{\partial t} v_h dx &= \sum_i \int_{K_i} \frac{\partial u_h}{\partial t} v_h dx \\ &= \sum_i \left(\sum_{\alpha=1}^{k+1} \omega_{\alpha} \frac{\partial u_h}{\partial t}(\hat{x}_i^{\alpha}) v_h(\hat{x}_i^{\alpha}) h + \mathcal{O}(h^{2k+1}) \right) \\ &= \sum_i \left(\sum_{\alpha=1}^{k+1} \omega_{\alpha} \frac{\partial U(u_h)}{\partial t}(\hat{x}_i^{\alpha}) h + \mathcal{O}(h^{2k+1}) \right) \\ &= \frac{d}{dt} \int_{\Omega} U(u_h) dx + \mathcal{O}(h^{2k}). \end{aligned}$$

Here, ω_{α} and \hat{x}_i^{α} are the Gauss-Lobatto weights and quadrature points in each cell K_i ,

with $\hat{x}_i^1 = x_{i-1/2}$ and $\hat{x}_i^{k+1} = x_{i+1/2}$. This indicates that the entropy can be considered stable, with only a small, high order growth. Also see [15].

Next, we present the prior error estimate for the linear scalar conservation law with $f(u) = u$. Let us recall some useful inequalities. For a piecewise polynomial $w \in V_h^k$, we have the inverse inequality

$$\left\| \frac{\partial w}{\partial x} \right\|_{L^2(K_i)} \lesssim h^{-1} \|w\|_{L^2(K_i)}, \quad \|w\|_{L^\infty(K_i)} \lesssim h^{-1/2} \|w\|_{L^2(K_i)}, \quad \forall K_i \in \mathcal{K}. \quad (2.22)$$

And for a given function u , its Gauss-Radau projection $P^-u \in V_h^k$ is uniquely defined by

$$\begin{cases} \int_{K_i} (P^-u - u)w \, dx = 0, & \forall w \in P^{k-1}(K_i), \\ P^-u(x_{i+1/2}^-) = u(x_{i+1/2}^-). \end{cases} \quad (2.23)$$

Assume $u \in H^{k+1}(\Omega)$, then the Gauss-Radau projection P^-u satisfies the error estimate [9]

$$|P^-u - u|_{m, K_i} \lesssim h^{k+1-m} \|u\|_{k+1, K_i} \quad (2.24)$$

for all $K_i \in \mathcal{K}$ and $0 \leq m \leq k$. Here, $|\cdot|_{m, K}$ and $\|\cdot\|_{m, K}$ denote the Sobolev (semi-)norms

$$|u|_{m, K} = \left(\int_K \left(\frac{\partial^m u}{\partial x^m} \right)^2 dx \right)^{1/2}, \quad \|u\|_{m, K} = \left(\sum_{l=0}^m \int_K \left(\frac{\partial^l u}{\partial x^l} \right)^2 dx \right)^{1/2}.$$

Now we give an error estimate of our scheme.

Theorem 2.3. (Error Estimate) Suppose u is a smooth solution of (2.1) with periodic or compactly supported boundary conditions. Consider equation (2.1) with linear flux $f(u) = u$ and square entropy $U = u^2/2$. If the initial data is chosen by the standard L^2 projection of $u_0(x)$, i.e.,

$$\int_{K_i} u_h(x, 0) \phi(x) dx = \int_{K_i} u_0(x) \phi(x) dx, \quad \forall K_i \in \mathcal{K}, \phi \in V_h^k,$$

then the numerical solution u_h of NOES-DG scheme (2.9) with the fluxes (2.13)-(2.14) satisfies

$$\|u(\cdot, t) - u_h(\cdot, t)\|_{L^2(\Omega)} \lesssim h^{k+1}. \quad (2.25)$$

Proof. Introduce a short-hand notation

$$B_i(u_h, w) = \int_{K_i} \frac{\partial u_h}{\partial t} w \, dx - \int_{K_i} u_h \frac{\partial w}{\partial x} dx + u_h|_{i+1/2}^- w_{i+1/2}^- - u_h|_{i-1/2}^- w_{i-1/2}^+,$$

then the scheme (2.9) can be written as

$$B_i(u_h, w) = -\sigma_i \int_{K_i} \nu_i \frac{\partial u_h}{\partial x} \frac{\partial w}{\partial x} dx, \quad \forall w \in V_h^k, K_i \in \mathcal{K}$$

On the other hand, the exact solution u satisfies

$$B_i(u, w) = 0, \quad \forall w \in V_h^k, K_i \in \mathcal{K}.$$

Hence,

$$B_i(u - u_h, w) = \sigma_i \int_{K_i} \nu_i \frac{\partial u_h}{\partial x} \frac{\partial w}{\partial x} dx, \quad \forall w \in V_h^k, K_i \in \mathcal{K}. \quad (2.26)$$

Denote

$$\varepsilon_h = u - P^-u, \quad e_h = P^-u - u_h \in V_h^k.$$

Taking $w = e_h$, (2.26) becomes

$$B_i(e_h, e_h) + \sigma_i \int_{K_i} \nu_i \left(\frac{\partial e_h}{\partial x} \right)^2 dx = -B_i(\varepsilon_h, e_h) + \sigma_i \int_{K_i} \nu_i \frac{\partial(P^-u)}{\partial x} \frac{\partial e_h}{\partial x} dx. \quad (2.27)$$

Since $\sigma_i \geq 0$, utilizing the periodic or compactly supported boundary conditions, we have that

$$\begin{aligned} & \sum_i \left(B_i(e_h, e_h) + \sigma_i \int_{K_i} \nu_i \left(\frac{\partial e_h}{\partial x} \right)^2 dx \right) \\ & \geq \sum_i \left(\int_{K_i} \frac{\partial e_h}{\partial t} e_h dx - \int_{K_i} e_h \frac{\partial e_h}{\partial x} dx + \left(e_h|_{i+1/2}^- \right)^2 - \left(e_h|_{i-1/2}^- \right) \left(e_h|_{i-1/2}^+ \right) \right) \\ & = \frac{1}{2} \frac{d}{dt} \int_{\Omega} (e_h)^2 dx + \sum_i \left(-\frac{1}{2} \left(e_h|_{i+1/2}^- \right)^2 + \frac{1}{2} \left(e_h|_{i-1/2}^+ \right)^2 + \left(e_h|_{i+1/2}^- \right)^2 - \left(e_h|_{i-1/2}^- \right) \left(e_h|_{i-1/2}^+ \right) \right) \\ & = \frac{1}{2} \frac{d}{dt} \int_{\Omega} (e_h)^2 dx + \sum_i \left(\frac{1}{2} \left(e_h|_{i-1/2}^- \right)^2 + \frac{1}{2} \left(e_h|_{i-1/2}^+ \right)^2 - \left(e_h|_{i-1/2}^- \right) \left(e_h|_{i-1/2}^+ \right) \right) \\ & = \frac{1}{2} \frac{d}{dt} \int_{\Omega} (e_h)^2 dx + \sum_i \frac{1}{2} \left(e_h|_{i-1/2}^- - e_h|_{i-1/2}^+ \right)^2 \\ & \geq \frac{1}{2} \frac{d}{dt} \int_{\Omega} (e_h)^2 dx. \end{aligned}$$

On the other hand, using the property of Gauss-Radau projection, we have that

$$\begin{aligned}
B_i(\varepsilon_h, e_h) &= \int_{K_i} \frac{\partial \varepsilon_h}{\partial t} e_h dx - \int_{K_i} \varepsilon_h \frac{\partial e_h}{\partial x} dx + \left(\varepsilon_h|_{i+1/2}^- \right) \left(e_h|_{i+1/2}^- \right) - \left(\varepsilon_h|_{i-1/2}^- \right) \left(e_h|_{i-1/2}^+ \right) \\
&= \int_{K_i} \frac{\partial \varepsilon_h}{\partial t} e_h dx.
\end{aligned}$$

Therefore,

$$\frac{1}{2} \frac{d}{dt} \int_{\Omega} (e_h)^2 dx \leq - \int_{\Omega} \frac{\partial \varepsilon_h}{\partial t} e_h dx + \sum_i \sigma_i \int_{K_i} \nu_i \frac{\partial(P^-u)}{\partial x} \frac{\partial e_h}{\partial x} dx.$$

For the last term, we have

$$\begin{aligned}
\sum_i \sigma_i \int_{K_i} \nu_i \frac{\partial(P^-u)}{\partial x} \frac{\partial e_h}{\partial x} dx &\leq \sum_i \sigma_i \left\| \frac{\partial(P^-u)}{\partial x} \right\|_{L^2(K_i)} \left\| \frac{\partial e_h}{\partial x} \right\|_{L^2(K_i)} \\
&\lesssim \sum_i \sigma_i h^{-1/2} \|e_h\|_{L^2(K_i)} \\
&\lesssim \left(\sum_i (\sigma_i)^2 h^{-1} \right)^{1/2} \|e_h\|_{L^2(\Omega)}.
\end{aligned}$$

In the second inequality, we have used the error estimate

$$\begin{aligned}
\left\| \frac{\partial(P^-u)}{\partial x} \right\|_{L^2(K_i)} &= |P^-u|_{1,K_i} \leq |u|_{1,K_i} + |u - P^-u|_{1,K_i} \\
&\lesssim |u|_{1,K_i} + h^k \|u\|_{k+1,K_i} \lesssim h^{1/2}.
\end{aligned}$$

For σ_i , since u is smooth, we have $|\partial_x^l u_h| = |[\partial_x^l(u - u_h)]|$. According to (2.15), the viscosity coefficient has an upper bound $\sigma_i \leq C\sigma_i^{jump}$. Hence,

$$\begin{aligned}
\sum_i (\sigma_i)^2 h^{-1} &\lesssim h \sum_i \sum_{l=0}^k \|[\partial_x^l u_h]\|_{\partial K_i}^2 h^{2l} \\
&= h \sum_i \sum_{l=0}^k \|[\partial_x^l (u - u_h)]\|_{\partial K_i}^2 h^{2l} \\
&\lesssim \sum_i \sum_{l=0}^k \|\partial_x^l e_h\|_{L^2(K_i)}^2 h^{2l} + \sum_i \sum_{l=0}^k \|\partial_x^l \varepsilon_h\|_{L^2(K_i)}^2 h^{2l} \\
&\lesssim \left(\|e_h\|_{L^2(\Omega)}^2 + h^{2k+2} \right).
\end{aligned}$$

Then (2.27) yields

$$\frac{1}{2} \frac{d}{dt} \int_{\Omega} (e_h)^2 dx \lesssim \left(\int_{\Omega} (e_h)^2 dx + h^{2k+2} \right)$$

Using the Gronwall's inequality, we can get that

$$\|e_h(\cdot, t)\|_{L^2(\Omega)} \lesssim \|e_h(\cdot, 0)\|_{L^2(\Omega)} + h^{k+1}.$$

Since $u_h(\cdot, 0)$ is obtained by the standard L^2 projection of u , resulting $\|(u - u_h)(\cdot, 0)\| \lesssim h^{k+1}$, thus $\|e_h(\cdot, 0)\| \lesssim h^{k+1}$. Finally, we can obtain that

$$\|u(\cdot, t) - u_h(\cdot, t)\|_{L^2(\Omega)} \lesssim h^{k+1}.$$

□

Remark 2.4. For arbitrary entropy function $U(u)$, if we assume $\partial_x^l u_h \lesssim 1$, $l = 0, 1, \dots, k$, and $A^{(k)}(u)$ is continuous with u , then the error estimate (2.25) still holds. We give a brief proof of this case under the assumptions. For a general $U(u)$, (2.26) is changed to

$$B_i(u - u_h, w) = \sigma_i \int_{K_i} \nu_i \frac{\partial v_h}{\partial x} A(u_h) \frac{\partial w}{\partial x} dx, \quad \forall w \in V_h^k, K_i \in \mathcal{K},$$

deriving that

$$B_i(e_h, e_h) = -B_i(\varepsilon_h, e_h) + \sigma_i \int_{K_i} \nu_i \frac{\partial v_h}{\partial x} A(u_h) \frac{\partial e_h}{\partial x} dx.$$

With the help of monotone numerical fluxes, we still have $\sum_i B_i(e_h, e_h) \geq \frac{1}{2} \frac{d}{dt} \int_{\Omega} (e_h)^2 dx$. Consequently,

$$\frac{1}{2} \frac{d}{dt} \int_{\Omega} (e_h)^2 dx \leq \int_{\Omega} \frac{\partial \varepsilon_h}{\partial t} e_h dx + \sum_i \sigma_i \int_{K_i} \nu_i \frac{\partial v_h}{\partial x} A(u_h) \frac{\partial e_h}{\partial x} dx.$$

It can be calculated that

$$\begin{aligned} & \sum_i \sigma_i \int_{K_i} \nu_i \frac{\partial v_h}{\partial x} A(u_h) \frac{\partial e_h}{\partial x} dx \\ &= \sum_i \sigma_i \int_{K_i} \nu_i \left[\left(\frac{\partial v_h}{\partial x} A(u_h) - \frac{\partial u_h}{\partial x} \right) + \frac{\partial u_h}{\partial x} \right] \frac{\partial e_h}{\partial x} dx \\ &\leq \sum_i \sigma_i \left(\left\| \frac{\partial v_h}{\partial x} A(u_h) - \frac{\partial u_h}{\partial x} \right\|_{L^2(K_i)} + \left\| \frac{\partial u_h}{\partial x} \right\|_{L^2(K_i)} \right) \left\| \frac{\partial e_h}{\partial x} \right\|_{L^2(K_i)}. \end{aligned}$$

According to the assumption and the definition that v_h is the $(k+1)$ -th interpolation of

$v(u_h)$, we have

$$\begin{aligned}
\left\| \frac{\partial v_h}{\partial x} A(u_h) - \frac{\partial u_h}{\partial x} \right\|_{L^2(K_i)} &= \left\| \frac{\partial v_h}{\partial x} A(u_h) - \frac{\partial v(u_h)}{\partial x} A(u_h) \right\|_{L^2(K_i)} \\
&\leq \max_{x \in K_i} |A(u_h)| \left\| \frac{\partial v_h}{\partial x} - \frac{\partial v(u_h)}{\partial x} \right\|_{L^2(K_i)} \\
&\lesssim \max_{x \in K_i} |A(u_h)| \max_{x \in K_i} \left| \frac{\partial^{k+1} v(u_h)}{\partial x^{k+1}} \right| h^{k+1/2} \\
&\lesssim h^{k+1/2}
\end{aligned}$$

and

$$\left\| \frac{\partial u_h}{\partial x} \right\|_{L^2(K_i)} \lesssim h^{1/2}.$$

Therefore, there still holds

$$\sum_i \sigma_i \int_{K_i} \nu_i \frac{\partial v_h}{\partial x} A(u_h) \frac{\partial e_h}{\partial x} dx \lesssim \left(\sum_i (\sigma_i)^2 h^{-1} \right)^{1/2} \|e_h\|_{L^2(\Omega)}.$$

The rest of the proof are similar.

2.2 1D system

Next, we consider the one-dimensional system

$$\mathbf{u}_t + \mathbf{f}(\mathbf{u})_x = \mathbf{0}. \quad (2.28)$$

where $\mathbf{u} : \mathbb{R} \rightarrow \mathbb{R}^p$ and $\mathbf{f} : \mathbb{R}^p \rightarrow \mathbb{R}^p$. For systems, we can also define the entropy pair (U, F) , which are still scalar functions with respect to \mathbf{u} and satisfy $U'(\mathbf{u})\mathbf{f}'(\mathbf{u}) = F'(\mathbf{u})$. Moreover, denote

$$\mathbf{v} = \left(\frac{\partial U}{\partial \mathbf{u}} \right)^T \in \mathbb{R}^p, \quad \mathbf{A}(\mathbf{u}) = \left(\frac{\partial^2 U}{\partial \mathbf{u}^2} \right)^{-1} \in \mathbb{R}^{p \times p}, \quad \mathbf{B}(\mathbf{v}) = \frac{\partial \mathbf{f}(\mathbf{u}(\mathbf{v}))}{\partial \mathbf{v}} \in \mathbb{R}^{p \times p}.$$

A strictly convex function U serves as an entropy function if and only if \mathbf{A} is a symmetric, positive-definite matrix and \mathbf{B} is symmetric. Furthermore, as mentioned in [7], the change of variables $\mathbf{u} \mapsto \mathbf{v}$ should symmetrize the viscous term simultaneously such that the entropy conditions could meet the vanishing viscosity approach.

For example, we consider the compressible Euler equation

$$\begin{bmatrix} \rho \\ \rho u \\ \mathcal{E} \end{bmatrix}_t + \begin{bmatrix} \rho u \\ \rho u^2 + p \\ u(\mathcal{E} + p) \end{bmatrix}_x = \mathbf{0}. \quad (2.29)$$

Here ρ , u and p are the density, velocity and pressure of the gas. \mathcal{E} is the total energy, satisfying the equation of state for polytropic ideal gas

$$\mathcal{E} = \frac{p}{\gamma - 1} + \frac{1}{2}\rho u^2, \quad \gamma = 1.4.$$

The physical specific entropy is $s = \ln(p\rho^{-\gamma})$. Harten [19] proved that there exists a family of entropy pairs that are related to s and satisfy the symmetric conditions. However, if we also want to symmetrize the viscous term in the compressible Navier–Stokes equations with heat conduction [22], there is only one choice of the entropy pair

$$U = -\frac{\rho s}{\gamma - 1}, \quad F = -\frac{\rho u s}{\gamma - 1}.$$

Correspondingly,

$$\mathbf{v} = \begin{bmatrix} \frac{\gamma - s}{\gamma - 1} - \frac{\rho u^2}{2p} \\ \rho u/p \\ -\rho/p \end{bmatrix},$$

$$\mathbf{A} = \begin{bmatrix} \rho & m & \frac{p}{\gamma - 1} + \frac{m^2}{2\rho} \\ m & p + \frac{m^2}{\rho} & \frac{m}{2\rho^2} \left(m^2 + \frac{2\gamma\rho p}{\gamma - 1} \right) \\ \frac{p}{\gamma - 1} + \frac{m^2}{2\rho} & \frac{m}{2\rho^2} \left(m^2 + \frac{2\gamma\rho p}{\gamma - 1} \right) & \frac{1}{4\rho^3} \left(m^4 + \frac{4\gamma m^2 \rho p}{\gamma - 1} + \frac{4\gamma \rho^2 p^2}{(\gamma - 1)^2} \right) \end{bmatrix},$$

with $m = \rho u$.

To construct the NOES-DG scheme, the corresponding viscosity equation in cell K_i is given as

$$\mathbf{u}_t + \mathbf{f}(\mathbf{u})_x = \sigma_i(\nu_i(x) \mathbf{A}(\mathbf{u})\mathbf{v}_x)_x, \quad (2.30)$$

Here, $\sigma_i \geq 0$ is scalar and $\nu_i(x)$ is defined the same as (2.8).

Then, the NOES-DG scheme of the system (2.28) is: find $\mathbf{u}_h \in [V_h^k]^p$, such that for

all $\mathbf{w} \in [V_h^k]^p$ and $K_i \in \mathcal{K}$,

$$\begin{aligned} \int_{K_i} \frac{\partial \mathbf{u}_h}{\partial t} \cdot \mathbf{w} dx &= \int_{K_i} \mathbf{f}(\mathbf{u}_h) \cdot \frac{\partial \mathbf{w}}{\partial x} dx - \hat{\mathbf{f}}_{i+1/2} \cdot \mathbf{w}_{i+1/2}^- + \hat{\mathbf{f}}_{i-1/2} \cdot \mathbf{w}_{i-1/2}^+ \\ &\quad - \sigma_i \int_{K_i} \nu_i(x) \left(\frac{\partial \mathbf{v}_h}{\partial x} \right)^T \mathbf{A}(\mathbf{u}_h) \frac{\partial \mathbf{w}}{\partial x} dx. \end{aligned} \quad (2.31)$$

Note that \mathbf{v}_h must interpolate the value of $\mathbf{v}(\mathbf{u}_h)$ at the interfaces, i.e.

$$\mathbf{v}_h|_{i+1/2}^- = \mathbf{v}(\mathbf{u}_h|_{i+1/2}^-), \quad \mathbf{v}_h|_{i-1/2}^+ = \mathbf{v}(\mathbf{u}_h|_{i-1/2}^+).$$

We do interpolation on each component based on the Gauss-Lobatto quadrature points again. The parameter σ_i is determined by $\sigma_i = \max \{ \sigma_i^{jump}, \sigma_i^{entropy} \}$ as well, where

$$\begin{aligned} \sigma_i^{jump} &= \max_{1 \leq m \leq p} \sigma_{i,m}^{jump}, \\ \sigma_{i,m}^{jump} &= c_f \left(h \| [u_{h,m}] \|_{\partial K_i} + \sum_{l=1}^k l(l+1) h^{l+1} \| [\partial_x^l u_{h,m}] \|_{\partial K_i} \right), \\ \sigma_i^{entropy} &= \min \left\{ \max \left\{ \frac{F_i}{E_i}, 0 \right\}, C \max_m \{ \sigma_{i,m}^{jump} \} \right\}, \\ E_i &= \int_{K_i} \nu_i(x) \left(\frac{\partial \mathbf{v}_h}{\partial x} \right)^T \mathbf{A}(\mathbf{u}_h) \frac{\partial \mathbf{v}_h}{\partial x} dx, \\ F_i &= \hat{F}_{i+1/2} - \hat{F}_{i-1/2} - \hat{\mathbf{f}}_{i+1/2}^C \cdot \mathbf{v}_h|_{i+1/2}^- + \hat{\mathbf{f}}_{i-1/2}^C \cdot \mathbf{v}_h|_{i-1/2}^+ + \int_{K_i} \mathbf{f}(\mathbf{u}_h) \cdot \frac{\partial \mathbf{v}_h}{\partial x} dx. \end{aligned}$$

Here, we define σ_i^{jump} measuring discontinuity on each component without characteristic decomposition. The numerical entropy flux \hat{F} is given as the central flux (2.13) as well. The numerical flux $\hat{\mathbf{f}} = \hat{\mathbf{f}}(\mathbf{u}_L, \mathbf{u}_R)$ is splitted into the central part $\hat{\mathbf{f}}^C$ and the diffusive part $\hat{\mathbf{f}}^D$. For example, for the Lax-Friedrichs flux,

$$\hat{\mathbf{f}}^C = \frac{1}{2} (\mathbf{f}(\mathbf{u}_L) + \mathbf{f}(\mathbf{u}_R)), \quad \hat{\mathbf{f}}^D = -\frac{\alpha}{2} (\mathbf{u}_R - \mathbf{u}_L), \quad \alpha = \max_{\mathbf{u}, i} \left| \lambda_i \left(\frac{\partial \mathbf{f}}{\partial \mathbf{u}} \right) \right|,$$

where λ_i is the i -th eigenvalue of the given matrix. For Euler equations, we can also take the numerical flux $\hat{\mathbf{f}}$ as HLL/HLLC flux [38]. Correspondingly, for HLL flux, we can set

$$\hat{\mathbf{f}}^C = \begin{cases} \mathbf{f}(\mathbf{u}_L), & S_L \geq 0, \\ \frac{S_L \mathbf{f}(\mathbf{u}_R) - S_R \mathbf{f}(\mathbf{u}_L)}{S_R - S_L}, & S_L < 0 < S_R, \\ \mathbf{f}(\mathbf{u}_R), & S_R \leq 0, \end{cases} \quad \hat{\mathbf{f}}^D = \begin{cases} 0, & S_L \geq 0, \\ \frac{S_R S_L (\mathbf{u}_R - \mathbf{u}_L)}{S_R - S_L}, & S_L < 0 < S_R, \\ 0, & S_R \leq 0, \end{cases}$$

where S_R and S_L are the local estimates of maximal and minimal wave speed at the interface, respectively. And for HLLC flux, we can set

$$\hat{\mathbf{f}}^C = \hat{\mathbf{f}} - \hat{\mathbf{f}}^D, \quad \hat{\mathbf{f}}^D = \begin{cases} 0, & S_L \geq 0, \\ \frac{S_* S_L (\mathbf{u}_R - \mathbf{u}_L)}{S_* - S_L}, & S_L < 0 \leq S_*, \\ \frac{S_R S_* (\mathbf{u}_R - \mathbf{u}_L)}{S_R - S_*}, & S_* < 0 < S_R, \\ 0, & S_R \leq 0, \end{cases}$$

where S_* is an estimate of contact wave speed calculated by $\mathbf{u}_R, \mathbf{u}_L, S_R, S_L$. The specific formula of $\hat{\mathbf{f}}$ and S_* can be found in [38].

Following the same idea in Theorem 2.2, we can also prove that scheme (2.31) is entropy stable for hyperbolic systems (2.28) with periodic or compact boundaries under the condition

$$\sigma_i^{entropy} < C \max_m \{\sigma_{i,m}^{jump}\}, \quad \forall K_i \in \mathcal{K}.$$

2.3 Two-dimensional system

In this section, we consider a two-dimensional system

$$\begin{cases} \mathbf{u}_t + \nabla \cdot \mathbf{f}(\mathbf{u}) = \mathbf{0}, & \mathbf{x} \in \Omega \subset \mathbb{R}^2, \\ \mathbf{u}(\mathbf{x}, 0) = \mathbf{u}_0(\mathbf{x}), \end{cases} \quad (2.32)$$

with

$$\mathbf{u} : \mathbb{R}^2 \rightarrow \mathbb{R}^p, \quad \mathbf{f}(\mathbf{u}) = (\mathbf{f}_1(\mathbf{u}), \mathbf{f}_2(\mathbf{u})) : \mathbb{R}^p \rightarrow \mathbb{R}^{p \times 2}.$$

Here, we consider the domain is a rectangular $\Omega = [a_x, b_x] \times [a_y, b_y]$ with either periodic or compact support in each direction. The entropy pair (U, \mathcal{F}) , where $\mathcal{F} = (F_1, F_2)$, should also satisfying the symmetric condition.

Assume the computational domain Ω is divided into a Cartesian mesh $\mathcal{K} = \{K_{ij} : K_{ij} = [x_{i-1/2}, x_{i+1/2}] \times [y_{j-1/2}, y_{j+1/2}]\}$. And the finite element space is defined as piecewise Q^k polynomial

$$V_h^k = \{w(x, y) : w(x, y)|_{K_{ij}} \in Q^k(K), \forall K_{ij} \in \mathcal{K}\}.$$

Then, the one-dimensional framework could be directly applied to rectangular meshes through tensor product, with appropriate adjustment on the additional local viscosity in cell K .

In particular, the local viscosity form of (2.32) on a cell $K \in \mathcal{K}$ is defined as

$$\mathbf{u}_t + \nabla \cdot \mathbf{f}(\mathbf{u}) = \sigma_K \nabla \cdot (\nu_K \mathbf{A}(\mathbf{u}) \nabla \mathbf{v}(\mathbf{u})). \quad (2.33)$$

We take

$$\nu_K(x, y) = (1 - X^2(x, y))(1 - Y^2(x, y)),$$

to satisfy the condition

$$\nu_K(\mathbf{x}) = 0, \quad \mathbf{x} \in \partial K, \quad \text{and} \quad \nu_K(\mathbf{x}) > 0, \quad \mathbf{x} \in K \setminus \partial K.$$

Here, $(x, y) \rightarrow (X, Y)$ is the map from physical cell K to the reference cell $K_0 = \{(X, Y) : -1 < X, Y < 1\}$.

The NOES-DG scheme of (2.32) reads: Find $\mathbf{u}_h \in [V_h^k]^p$, such that for all $\mathbf{w} \in [V_h^k]^p$ and $K \in \mathcal{K}$,

$$\begin{aligned} \int_K \mathbf{u}_h \cdot \mathbf{w} \, dK - \int_K \mathbf{f}(\mathbf{u}_h) : \nabla \mathbf{w} \, dK + \int_{\partial K} \hat{\mathbf{f}}(\mathbf{u}_h^{int}, \mathbf{u}_h^{ext}, \mathbf{n}) \cdot \mathbf{w} \, dS \\ = -\sigma_K \int_K \nu_K(\mathbf{A}(\mathbf{u}_h) \nabla \mathbf{v}_h) : \nabla \mathbf{w} \, dK. \end{aligned} \quad (2.34)$$

Here, $\hat{\mathbf{f}}$ is the numerical flux consistent with $\mathbf{f}(\mathbf{u}) \cdot \mathbf{n}$, and \mathbf{n} is the unit outer normal vector of K . We can take \mathbf{v}_h as the two-dimensional Gauss-Lobatto interpolation of $\mathbf{v}(\mathbf{u}_h)$ as well. Moreover, the parameter is given by $\sigma_K = \max\{\sigma_K^{jump}, \sigma_K^{entropy}\}$,

$$\begin{aligned} \sigma_K^{jump} &= \max_{1 \leq m \leq p} \sigma_{K,m}^{jump}, \\ \sigma_{K,m}^{jump} &= c_f \left(h_K \| [u_{h,m}] \|_{\partial K} + \sum_{|l|=1}^k |l| (|l| + 1) h_K^{|l|+1} \| [\partial^l u_{h,m}] \|_{\partial K} \right), \quad l \in \mathbb{N}^d, \\ \sigma_K^{entropy} &= \min \left\{ \max \left\{ \frac{F_K}{E_K}, 0 \right\}, C \max_m \{ \sigma_{K,m}^{jump} \} \right\}, \\ E_K &= \int_K \nu_K(\mathbf{A}(\mathbf{u}_h) \nabla \mathbf{v}_h) : \nabla \mathbf{v}_h \, dK \\ F_K &= \int_{\partial K} \hat{\mathcal{F}} \cdot \mathbf{n} \, dS - \int_{\partial K} (\hat{\mathbf{f}}^C \cdot \mathbf{n}) \cdot \mathbf{v}_h^{int} \, dS + \int_K \mathbf{f}(\mathbf{u}_h) : \nabla \mathbf{v}_h \, dK, \end{aligned} \quad (2.35)$$

where $\hat{\mathcal{F}} = (\hat{F}_1, \hat{F}_2)^T$.

In this paper, we consider the two-dimensional Euler equation, where

$$\mathbf{u} = \begin{bmatrix} \rho \\ \rho u \\ \rho v \\ \mathcal{E} \end{bmatrix}, \quad \mathbf{f}_1(\mathbf{u}) = \begin{bmatrix} \rho u \\ \rho u^2 + p \\ \rho uv \\ u(\mathcal{E} + p) \end{bmatrix}, \quad \mathbf{f}_2(\mathbf{u}) = \begin{bmatrix} \rho v \\ \rho uv \\ \rho v^2 + p \\ v(\mathcal{E} + p) \end{bmatrix}$$

with

$$\mathcal{E} = \frac{p}{\gamma - 1} + \frac{1}{2}\rho(u^2 + v^2), \quad \gamma = 1.4.$$

And the entropy pair is

$$U = -\frac{\rho s}{\gamma - 1}, \quad F_1 = -\frac{\rho us}{\gamma - 1}, \quad F_2 = -\frac{\rho vs}{\gamma - 1}.$$

Further,

$$\mathbf{v} = \begin{bmatrix} \frac{\gamma - s}{\gamma - 1} - \frac{\rho(u^2 + v^2)}{2p} \\ \rho u/p \\ \rho v/p \\ -\rho/p \end{bmatrix},$$

and

$$\mathbf{A} = \begin{bmatrix} \rho & m_1 & m_2 & \frac{p}{\gamma - 1} + \frac{M}{2\rho} \\ m_1 & p + \frac{m_1^2}{\rho} & \frac{m_1 m_2}{\rho} & \frac{m_1}{2\rho^2} \left(M + \frac{2\gamma \rho p}{\gamma - 1} \right) \\ m_2 & \frac{m_1 m_2}{\rho} & p + \frac{m_2^2}{\rho} & \frac{m_2}{2\rho^2} \left(M + \frac{2\gamma \rho p}{\gamma - 1} \right) \\ \frac{p}{\gamma - 1} + \frac{M}{2\rho} & \frac{m_1}{2\rho^2} \left(M + \frac{2\gamma \rho p}{\gamma - 1} \right) & \frac{m_2}{2\rho^2} \left(M + \frac{2\gamma \rho p}{\gamma - 1} \right) & A_{44} \end{bmatrix},$$

with

$$m_1 = \rho u, \quad m_2 = \rho v, \quad M = m_1^2 + m_2^2, \quad A_{44} = \frac{1}{4\rho^3} \left(M^2 + \frac{4\gamma M \rho p}{\gamma - 1} + \frac{4\gamma \rho^2 p^2}{(\gamma - 1)^2} \right).$$

The flux splitting formula is given along each direction, which is the same as that in 1D.

Remark 2.5. For triangular meshes, it is usually to use P^k basis in numerical im-

plementation. In this case we can also define \mathbf{v}_h interpolating $\mathbf{v}(\mathbf{u}_h)$ on Gauss-Lobatto points along the edges. In general, for a P^k polynomial we have $(k+1)(k+2)/2$ degrees of freedom, and the number of conditions of interpolation is $3k$. Therefore, the interpolation exists for all $k > 0$ and is unique for $k = 1, 2$. When $k > 2$, there are some extra degrees of freedom to be determined, we may let v_h interpolate some other points such as [20]. The method can also extend to other types of meshes, and it will be left to future work.

3 Fully discretization

3.1 Integral factor SSP-RK method

The PDE can be solved in the MOL framework, that is after DG discretization the semi-discrete scheme can be treated as an ODE system, and then, we can apply a known ODE solver on it to obtain the fully discrete scheme. However, for the numerical solution containing discontinuities, the additional viscous term is a stiff term, leading a very strictly limited time step when coupling with explicit time discretization. To avoid this problem, we will employ the integrating factor strong-stability-preserving Runge-Kutta (IF-SSP-RK) method introduced in [6]. Here, we only discuss the one-dimensional scalar case for simplify.

Suppose we take the Legendre polynomials $\{\phi_{i,l}\}$ as the basis functions of V_h^k in K_i , where $\phi_{i,l}$ is polynomials of degree l . Then, the numerical solution can be presented as

$$u_h(x, t)|_{K_i} = \sum_{l=0}^k u_i^l(t) \phi_{i,l}(x).$$

We align the coefficients as a vector

$$\mathbf{u}_h = (u_1^0, \dots, u_1^k, u_2^0, \dots, u_2^k, \dots, u_N^0, \dots, u_N^k)^T \in \mathbb{R}^{(k+1)N}.$$

After the DG spatial discretization, we obtain the following ODE system

$$\frac{d}{dt} \mathbf{u}_h = \mathcal{L}_h(\mathbf{u}_h) + \mathcal{L}_h^v(\mathbf{u}_h), \quad (3.36)$$

where $\mathcal{L}_h^v(\mathbf{u}_h)$ corresponding to the artificial viscosity, which may be a stiff term.

To introduce the IF-SSP-RK, we begin with a specific case that this stiff term is semilinear, i.e. $\mathcal{L}_h^v(\mathbf{u}_h) = \mathbf{C}\mathbf{u}_h$, where \mathbf{C} is a constant matrix. Then we can multiply the factor $e^{-\mathbf{C}t}$ on both sides and get that

$$\frac{d}{dt} (e^{-\mathbf{C}t} \mathbf{u}_h) = e^{-\mathbf{C}t} \mathcal{L}_h(\mathbf{u}_h).$$

Then the IF-SSP-RK schemes can be obtained via applying RK scheme on the above ODE. In particular, the third-order IF-SSP-RK method [6] is given as following

$$\begin{aligned}\mathbf{u}_h^{(1)} &= \frac{1}{2}e^{\frac{2}{3}\mathbf{C}\Delta t} \left(2\mathbf{u}_h^n + \frac{4}{3}\Delta t \mathcal{L}_h(\mathbf{u}_h^n) \right), \\ \mathbf{u}_h^{(2)} &= \frac{2}{3}e^{\frac{2}{3}\mathbf{C}\Delta t} \mathbf{u}_h^n + \frac{1}{3} \left(\mathbf{u}_h^{(1)} + \frac{4}{3}\Delta t \mathcal{L}_h(\mathbf{u}_h^{(1)}) \right), \\ \mathbf{u}_h^{n+1} &= \frac{59}{129}e^{\mathbf{C}\Delta t} \mathbf{u}_h^n + \frac{15}{129}e^{\mathbf{C}\Delta t} \left(\mathbf{u}_h^n + \frac{4}{3}\Delta t \mathcal{L}_h(\mathbf{u}_h^n) \right) + \frac{27}{64} \left(\mathbf{u}_h^{(2)} + \frac{4}{3}\Delta t \mathcal{L}_h(\mathbf{u}_h^{(2)}) \right).\end{aligned}\tag{3.37}$$

If the stiff term is nonlinear, we can use $\mathbf{C}_n \mathbf{u}_h$ to approximate $\mathcal{L}_h^v(\mathbf{u}_h)$, where \mathbf{C}_n is a constant matrix. Then, rewrite the ODE system (3.36) as

$$\frac{d}{dt} \mathbf{u}_h = \mathcal{L}_h(\mathbf{u}_h) + \mathcal{L}_h^v(\mathbf{u}_h) - \mathbf{C}_n \mathbf{u}_h + \mathbf{C}_n \mathbf{u}_h.\tag{3.38}$$

Denote $\tilde{\mathcal{L}}_h(\mathbf{u}_h) := \mathcal{L}_h(\mathbf{u}_h) + \mathcal{L}_h^v(\mathbf{u}_h) - \mathbf{C}_n \mathbf{u}_h$. Then we can get the fully-discrete scheme via the same processing replacing $\mathcal{L}_h(\mathbf{u}_h)$ and \mathbf{C} in (3.37) by $\tilde{\mathcal{L}}_h(\mathbf{u}_h)$ and \mathbf{C}_n respectively.

Notice that in our scheme, the viscosity term $\int_{K_i} \nu_i(x)(v_h)_x A(u_h) w_x dx$ is a nonlinear local form. To choose a simple form of \mathbf{C}_n , we first consider a special case with square entropy $U(u) = u^2/2$, and denote the corresponding matrix \mathbf{C}_n as \mathbf{C}_n^{square} . In this case $A(u_h)(v_h)_x = (u_h)_x$ and the matrix \mathbf{C}_n^{square} can be given exactly satisfying $\mathbf{C}_n^{square} \mathbf{u}_h = \mathcal{L}_h^v(\mathbf{u}_h)$. To be specific, according to the local property, \mathbf{C}_n^{square} is a blocked diagonal matrix. Additionally, with the function $\nu_i(x) = 1 - X_i^2(x)$, the basis function $\phi_{i,l}$ satisfies a Sturm-Liouville equation

$$\frac{h^2}{4} \frac{d}{dx} \left(\nu_i \frac{d}{dx} \phi_{i,l} \right) + l(l+1) \phi_{i,l} = 0,$$

leading to

$$\int_{K_i} \nu_i (\phi_{i,l})_x (\phi_{i,q})_x dx = \delta_{lq} \frac{2}{h} l(l+1) m_l, \quad m_l = \frac{2}{2l+1} \left(\frac{2^l (l!)^2}{(2l)!} \right)^2.$$

Therefore, we can derive that \mathbf{C}_n^{square} is a diagonal matrix

$$\mathbf{C}_n^{square} = \frac{1}{h^2} \text{diag} \{ \sigma_1, \sigma_2, \dots, \sigma_N \} \otimes \text{diag} \{ 0, 4, \dots, 2k(k+1) \},\tag{3.39}$$

where \otimes is the Kronecker product $\mathbf{A} \otimes \mathbf{B} = (a_{ij} \mathbf{B})$. For a general entropy function U , since $A(u_h)(v_h)_x \approx (u_h)_x$, we can also set $\mathbf{C}_n = \mathbf{C}_n^{square}$ (3.39) in (3.38). As a consequence, the matrix $e^{\mathbf{C}_n \Delta t}$ can be obtained directly, making the algorithm easy to

implement.

3.2 Positivity-preserving limiter

For some extreme problems, the negative density or pressure may be introduced. If the density or pressure becomes negative, the system (2.28) will be non-hyperbolic and thus the initial value problem will be ill-posed. Here, we try to utilize the positivity-preserving (PP) limiter [41] to avoid this problem. However, our time discretization is different from the standard SSP-RK method, which is used in [41]. Hence, we need to reanalysis the limiter to match the IF-SSP-RK scheme.

Firstly, we give a brief review of the PP limiter [41] for one-dimensional Euler equation (2.28) based on the standard DG scheme coupling with the forward Euler time discretization

$$\int_{K_i} \frac{\mathbf{u}_h^{n+1} - \mathbf{u}_h^n}{\Delta t} \cdot \mathbf{w} dx - \int_{K_i} \mathbf{f}(\mathbf{u}_h^n) \cdot \frac{\partial \mathbf{w}}{\partial x} dx + \hat{\mathbf{f}}_{i+1/2}^n \mathbf{w}_{i+1/2}^- - \hat{\mathbf{f}}_{i-1/2}^n \mathbf{w}_{i-1/2}^+ = \mathbf{0}. \quad (3.40)$$

Let $\mathcal{G} \subset \mathbb{R}^3$ denote the admissible set

$$\mathcal{G} := \left\{ (\rho, m, \mathcal{E}) : \rho > 0 \text{ and } p = (\gamma - 1) \left(\mathcal{E} - \frac{1}{2} \frac{m^2}{\rho} \right) > 0 \right\}$$

which is convex. It was proved that the first order DG scheme ($k = 0$) is positivity preserving under a certain CFL condition $\frac{\Delta t}{h} \|(|u| + c)\|_{L^\infty(\Omega)} \leq \alpha_0$, that is if $\bar{\mathbf{u}}_i^n \in \mathcal{G}$, then $\bar{\mathbf{u}}_i^{n+1} \in \mathcal{G}$. Here, $\bar{\mathbf{u}}_i^n$ is the cell average of the numerical solution in the cell K_i at time t_n .

$$\bar{\mathbf{u}}_i^n = \frac{1}{h} \int_{K_i} \mathbf{u}_h(x, t^n) dx.$$

Moreover, [41] showed that the standard high order DG scheme can maintain $\bar{\mathbf{u}}_i^{n+1} \in \mathcal{G}$ under a suitable CFL condition, as long as the values of the approximation polynomials at the Gauss-Lobatto quadrature points belong to \mathcal{G} . Based on these conclusions, authors designed a PP limiter as a simplified linear scaling limiter, without destroying the original order of accuracy. Since a SSP-RK method is a convex combination of Euler steps, the positivity-preserving can still hold if we apply the limiter on each stage of SSP-RK methods.

In the following, we will design the PP-limiter on the NOES-DG scheme (2.31). Let $\{(\hat{x}_i^q, \omega_q)\}_{q=1}^{k+1}$ be the Gauss-Lobatto points and quadrature weights on a interval K_i . Note that the NOES-DG scheme coupling with Euler forward can generate the following form

$$\bar{\mathbf{u}}_i^{n+1} = \bar{\mathbf{u}}_i^n - \frac{\Delta t}{h} \cdot \left(\hat{\mathbf{f}}_{i+1/2}^n - \hat{\mathbf{f}}_{i-1/2}^n \right) := \bar{\mathbf{u}}_i^n + \Delta t \mathcal{L}_i^{ave}(\mathbf{u}_h^n),$$

which is the same as that of the traditional DG scheme. This tell us that the artificial

viscosity term does not affect the cell-averages. Hence, we can obtain the same conclusion for the NOES-DG scheme.

Theorem 3.1. *Consider the NOES-DG scheme coupling with Euler forward discretization. If the numerical solution \mathbf{u}_h^n satisfies*

$$\mathbf{u}_h^n(\hat{x}_i^q) \in \mathcal{G}, \quad \forall i, q. \quad (3.41)$$

Then $\bar{\mathbf{u}}_i^{n+1} \in \mathcal{G}$ under the CFL condition

$$\frac{\Delta t}{h} \|(|u| + c)\|_{L^\infty(\Omega)} \leq \omega_1 \alpha_0. \quad (3.42)$$

The proof is the same as that of the traditional DG scheme [41], which would not been repeated here.

Furthermore, based on the consistency of these two methods, we can utilized the the PP-limiter in [41] on our NOES-DG scheme to meet the condition (3.41), which is realized with the help of two scaling parameters $\theta_i^{(1)}, \theta_i^{(2)} \in [0, 1]$ on each cell K_i , and set

$$\begin{aligned} \tilde{\rho}_h^n|_{K_i} &= \left(1 - \theta_i^{(1)}\right) \bar{\rho}_i^n + \theta_i^{(1)} \rho_h^n|_{K_i}, \\ \left(\begin{array}{c} \rho_h \\ m_h \\ \mathcal{E}_h \end{array} \right)^{n, (mod)} \Big|_{K_i} &= \left(1 - \theta_i^{(2)}\right) \left(\begin{array}{c} \bar{\rho}_i^n \\ \bar{m}_i^n \\ \bar{\mathcal{E}}_i^n \end{array} \right) + \theta_i^{(2)} \left(\begin{array}{c} \tilde{\rho}_h \\ m_h \\ \mathcal{E}_h \end{array} \right)^n \Big|_{K_i} \end{aligned} \quad (3.43)$$

to guarantee $\tilde{\rho}_h^n(\hat{x}_i^q) \geq 0$ and $\mathbf{u}_h^{n, (mod)}(\hat{x}_i^q) \in \mathcal{G}$. To be specific, the value of θ is calculated by

$$\theta_i^{(1)} = \min \left\{ \frac{\bar{\rho}_i^n - \varepsilon}{\bar{\rho}_i^n - \rho_m}, 1 \right\}, \quad \rho_m = \min_{1 \leq q \leq k+1} \rho_h^n(\hat{x}_i^q), \quad (3.44)$$

$$\theta_i^{(2)} = \min_{1 \leq q \leq k+1} \{t_q\}, \quad t_q = \begin{cases} 1, & p(\tilde{\mathbf{u}}_h(\hat{x}_i^q)) \geq \varepsilon, \\ \tilde{t}_q, & p(\tilde{\mathbf{u}}_h(\hat{x}_i^q)) < \varepsilon, \end{cases} \quad (3.45)$$

where $\tilde{\mathbf{u}}_h = (\tilde{\rho}_h^n, m_h^n, \mathcal{E}_h^n)$, and \tilde{t}_q satisfies

$$p((1 - \tilde{t}_q)\bar{\mathbf{u}}_i + \tilde{t}_q\tilde{\mathbf{u}}_h(\hat{x}_i^q)) = \varepsilon$$

can be obtained by solving a nonlinear equation. The parameter ε is a small number, and we set $\varepsilon = 10^{-13}$ as the same in [41]. We want to remark that the scaling PP-limiter (3.43) does not change the cell average, and moreover, as showed in [41], it can maintain the original high order of accuracy for smooth solutions.

Next, we concern on the proposed NOES-DG scheme coupling with the IF-SSP-RK

scheme, and have the following conclusion.

Theorem 3.2. *Consider the NOES-DG scheme (2.31) with PP limiter (3.43) and IF-SSP-RK time discretization (3.37), then the numerical solution satisfies $\bar{\mathbf{u}}_i^{n+1} \in \mathcal{G}$ under the CFL condition*

$$\frac{\Delta t}{h} \|(|u| + c)\|_{L^\infty(\Omega)} \leq \frac{3}{4} \omega_1 \alpha_0. \quad (3.46)$$

Proof. We denote the PP limiter as an operator \mathcal{M} . Thus, the fully discrete scheme yields

$$\begin{aligned} \bar{\mathbf{u}}_i^{(1)} &= \frac{1}{2} \bar{\mathbf{u}}_i^n + \frac{1}{2} \left(\bar{\mathbf{u}}_i^n + \frac{4}{3} \Delta t \cdot \mathcal{L}_i^{ave} (\mathcal{M}(\mathbf{u}_h^n)) \right), \\ \bar{\mathbf{u}}_i^{(2)} &= \frac{2}{3} \bar{\mathbf{u}}_i^n + \frac{1}{3} \left(\bar{\mathbf{u}}_i^{(1)} + \frac{4}{3} \Delta t \cdot \mathcal{L}_i^{ave} (\mathcal{M}(\bar{\mathbf{u}}_h^{(1)})) \right), \\ \bar{\mathbf{u}}_i^{n+1} &= \frac{59}{129} \bar{\mathbf{u}}_i^n + \frac{15}{129} \left(\bar{\mathbf{u}}_i^n + \frac{4}{3} \Delta t \cdot \mathcal{L}_i^{ave} (\mathcal{M}(\mathbf{u}_h^n)) \right) + \frac{27}{64} \left(\bar{\mathbf{u}}_i^{(2)} + \frac{4}{3} \Delta t \cdot \mathcal{L}_i^{ave} (\mathcal{M}(\bar{\mathbf{u}}_h^{(2)})) \right). \end{aligned} \quad (3.47)$$

It can be seen that (3.47) is also a convex combination of Euler steps, but the time step is changed to $4\Delta t/3$. Since the PP limiter ensures $\mathcal{M}(\mathbf{u}_h^n)(\hat{x}_i^q) \in \mathcal{G}$ for each q , thus under the CFL condition (3.46), we have $\bar{\mathbf{u}}_i^{(1)} \in \mathcal{G}$. Likewise, we can further have $\bar{\mathbf{u}}_i^{(2)} \in \mathcal{G}$ and $\bar{\mathbf{u}}_i^{n+1} \in \mathcal{G}$. \square

Remark 3.1. *For the two-dimensional cases, the PP collocation of a rectangular cell is changed to $\mathbb{S}_{2D} = (\mathbb{S}_i^x \times \hat{\mathbb{S}}_j^y) \cup (\hat{\mathbb{S}}_i^x \times \mathbb{S}_j^y)$, where \mathbb{S}_i^x and $\hat{\mathbb{S}}_i^x$ denote the Gauss points and Gauss-Lobatto points on $[x_{i-1/2}, x_{i+1/2}]$, respectively. Then the scaling coefficients $\theta_{ij}^{(1)}, \theta_{ij}^{(2)}$ are calculated on these $2(k+1)^2$ points [41]. For triangular meshes, the main difference is of the scaling limiter points collocation, and the details can refer to [42].*

4 Numerical tests

In this section, we present the results of our numerical experiments for the schemes described in the previous sections. In particular, for smooth problems, we do accuracy test with $k = 1, 2, 3$. And for those non-smooth problems, without loss of generality, we only show results with $k = 2$. The domain is divided into uniform meshes. The third-order IF-SSP-RK method is used for time discretization, with time step

$$\Delta t = \frac{\text{CFL}}{\max\{\alpha_x, \alpha_y\}} h,$$

and CFL is taken as 0.2. Without special declaration, we take the parameter $C = 50$ for all tests. And c_f in σ_i^{jump} is defined as $c_f = c_0 \max_{\mathbf{x} \in K} \{|\nabla \cdot \mathbf{f}|\}$ and $c_f = c_0 \max_{\mathbf{x} \in K} \{1/H\}$ in cell K for scalar equations and Euler system respectively, where $H = (\mathcal{E} + p)/\rho$ denotes

the enthalpy. Time evolution of the total entropy will be given for some problems, which is defined as $\int_{\Omega} U(u_h)dx$.

4.1 One-dimensional tests

Example 4.1. (*Linear equation.*)

We first consider the linear equation

$$u_t + u_x = 0, \quad x \in \Omega = [0, 2\pi],$$

with periodic boundary conditions. The exact solution is $u(x, t) = u(x - t, 0)$. In this example, we choose the entropy function as $U(u) = e^u$.

First, we test the accuracy of the scheme with the smooth initial data $u(x, 0) = \sin(x)$. In Table 4.1, we present the errors and orders of accuracy at $T = 2\pi$. We can observe the optimal convergence rates for $k = 1, 2, 3$.

Next, we test this problem with the non-smooth initial data

$$u(x, 0) = \begin{cases} 1, & 0.5\pi < x < 1.5\pi, \\ 0, & \text{otherwise.} \end{cases}$$

In Figure 4.1, we present the result at $T = 2\pi$ with $N = 200$ cells. It can be seen that there is no obvious oscillation near the discontinuity, demonstrating that our proposed scheme can control spurious oscillation efficiently. The development of total entropy is shown in Figure 4.3(a), indicating that this quantity does not increase with time during the simulation.

Table 4.1. Example 4.1: One dimensional linear equation with smooth initial data. Errors and orders at final time $T = 2\pi$.

	N	L^1 error	order	L^2 error	order	L^∞ error	order
$k = 1$	64	3.39e-04	—	4.35e-04	—	1.09e-03	—
	128	8.09e-05	2.07	1.05e-04	2.06	3.05e-04	1.83
	256	1.99e-05	2.02	2.60e-05	2.01	7.96e-05	1.94
	512	4.94e-06	2.01	6.48e-06	2.00	2.02e-05	1.97
$k = 2$	64	4.38e-06	—	5.15e-06	—	1.27e-05	—
	128	3.90e-07	3.49	4.75e-07	3.44	1.29e-06	3.30
	256	4.65e-08	3.07	5.66e-08	3.07	1.57e-07	3.05
	512	5.75e-09	3.02	6.99e-09	3.02	1.95e-08	3.01
$k = 3$	64	6.13e-08	—	7.29e-08	—	1.60e-07	—
	128	1.98e-09	4.95	2.60e-09	4.81	6.30e-09	4.67
	256	1.08e-10	4.19	1.45e-10	4.16	3.82e-10	4.04
	512	7.10e-12	3.93	9.16e-12	3.98	2.27e-11	4.07

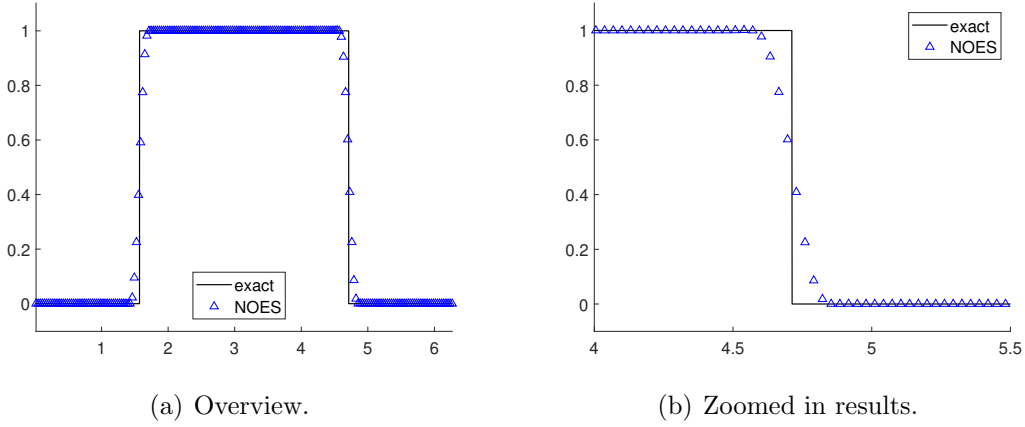


Figure 4.1. Example 4.1: one dimensional linear equation with non-smooth initial data. The numerical solution at $T = 2\pi$ with $N = 200$.

Example 4.2. (*Burgers' equation.*)

Here we consider the Burgers' equation

$$u_t + \left(\frac{u^2}{2} \right)_x = 0, \quad x \in \Omega = [0, 2\pi]$$

with periodic boundary conditions. The initial condition is given by $u(x, 0) = 0.5 + \sin x$. We choose the entropy function as $U(u) = e^u$.

We first compare the numerical results at the final time $T = 0.6$, when the solution is still smooth. The errors and orders of accuracy are presented in Table 4.2. Again, we can obtain the optimal convergence rate for all cases.

Moreover, in Figure 4.2, we present the results with $N = 200$ cells at final time $T = 2.2$, when the solution contains a discontinuity in Ω . We can see that our scheme captures the shock well without numerical oscillations. In Figure 4.3(b), we present the development of total entropy with time. It can be seen that the total entropy does not increasing.

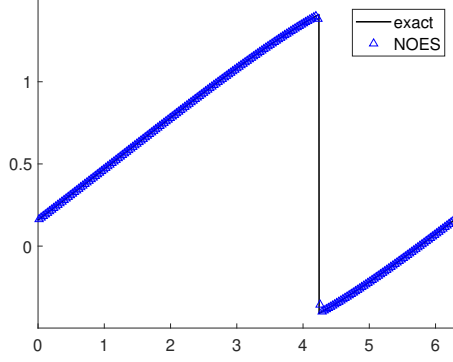
Example 4.3. (*Buckley-Leverett equation.*)

In this example, we consider the one-dimensional Buckley-Leverett equation

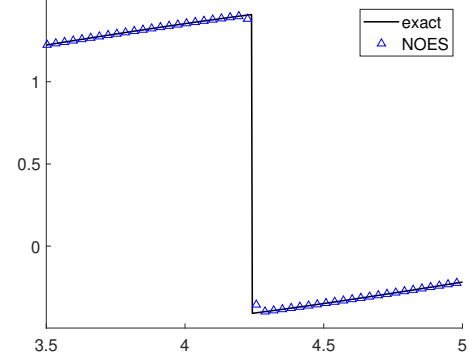
$$u_t + \left(\frac{4u^2}{4u^2 + (1-u)^2} \right)_x = 0$$

with a Riemann initial condition

$$u(x, 0) = \begin{cases} u_L, & x \leq 0, \\ u_R, & x > 0. \end{cases}$$

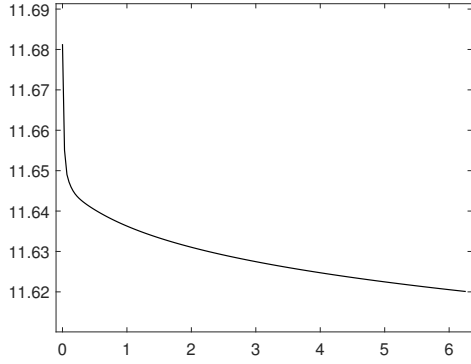


(a) Overview.

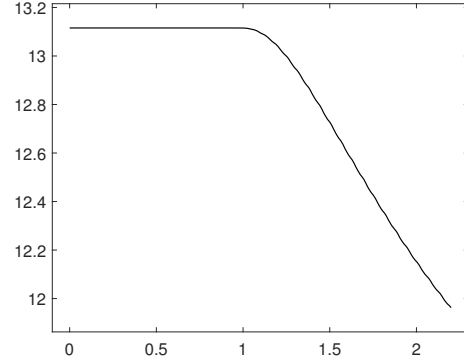


(b) Zoomed in results.

Figure 4.2. Example 4.2: One-dimensional Burgers' equation. The numerical solution at $T = 2.2$ with $N = 200$ cells.



(a) Linear equation.



(b) Burgers' equation.

Figure 4.3. One-dimensional tests: Evolution of the total entropy with time.

Table 4.2. Example 4.2: one-dimensional Burgers' equation. Errors and orders at final time $T = 0.6$.

	N	L^1 error	order	L^2 error	order	L^∞ error	order
$k = 1$	64	4.52e-04	–	8.12e-04	–	5.02e-03	–
	128	1.16e-04	1.97	2.14e-04	1.92	1.38e-03	1.86
	256	2.95e-05	1.97	5.56e-05	1.95	3.60e-04	1.94
	512	7.49e-06	1.98	1.42e-05	1.97	9.14e-05	1.98
$k = 2$	64	1.22e-05	–	3.22e-05	–	2.82e-04	–
	128	1.45e-06	3.08	3.84e-06	3.07	4.06e-05	2.80
	256	1.82e-07	2.99	4.87e-07	2.98	5.44e-06	2.90
	512	2.28e-08	3.00	6.17e-08	2.98	7.08e-07	2.94
$k = 3$	64	4.28e-07	–	1.41e-06	–	8.69e-06	–
	128	2.42e-08	4.15	8.30e-08	4.08	6.22e-07	3.80
	256	1.52e-09	3.99	5.38e-09	3.95	4.10e-08	3.92
	512	9.69e-11	3.98	3.46e-10	3.96	2.61e-09	3.97

This example is very challenging in computation because of the non-convexity of f . If the numerical schemes are not carefully designed, they may fail to converge to the unique entropy solution or may be too slow to converge [25]. The computational domain is $\Omega = [-0.5, 0.5]$. Following the setup in [30], we consider two kinds of initial conditions:

$$\text{IC1: } u_L = -3, u_R = 3,$$

$$\text{IC2: } u_L = 2, u_R = -2,$$

with three different entropy functions:

$$\text{U1: } U(u) = \frac{u^2}{2},$$

$$\text{U2: } U(u) = \int \arctan(20u) du,$$

$$\text{U3: } U(u) = \int \arctan(u - 1) du.$$

The first entropy function is the standard square entropy, the second one is a modified version of the Kruzhkov's entropy $U(u) = |u|$, and the third one is a modified version of the translated Kruzhkov's entropy $U(u) = |u - 1|$.

In Figure 4.4, we present the results at $T = 1$ with $N = 200$ cells. The reference solution is simulated by the fifth-order finite difference WENO scheme on 10000 cells. From these results, we can see that for IC1, scheme with U2 gives the best simulation. Meanwhile, for IC2, only scheme with U3 can provide the satisfactory results. This is consistent with the results in [7, 30]. The results indicate that carefully selecting the entropy function helps to obtain physically correct solutions, especially for the nonconvex

hyperbolic conservation laws.

Moreover, to demonstrate the efficacy of parameter σ in (2.9), we present the results for different settings for σ in Figure 4.5. We denote $\sigma_i = \sigma_i^{entropy}$ as "entropy", $\sigma_i = \sigma_i^{jump}$ as "jump", and the proposed NOES-DG scheme as "entropy + jump" in following. It can be seen that even for IC1 with U2, the solution is incorrect if we only concern the entropy term. And for IC2 with U3, the solution is incorrect when we only consider the jump term. These results show that two parameters, σ_i^{jump} and $\sigma_i^{entropy}$, are both necessary.

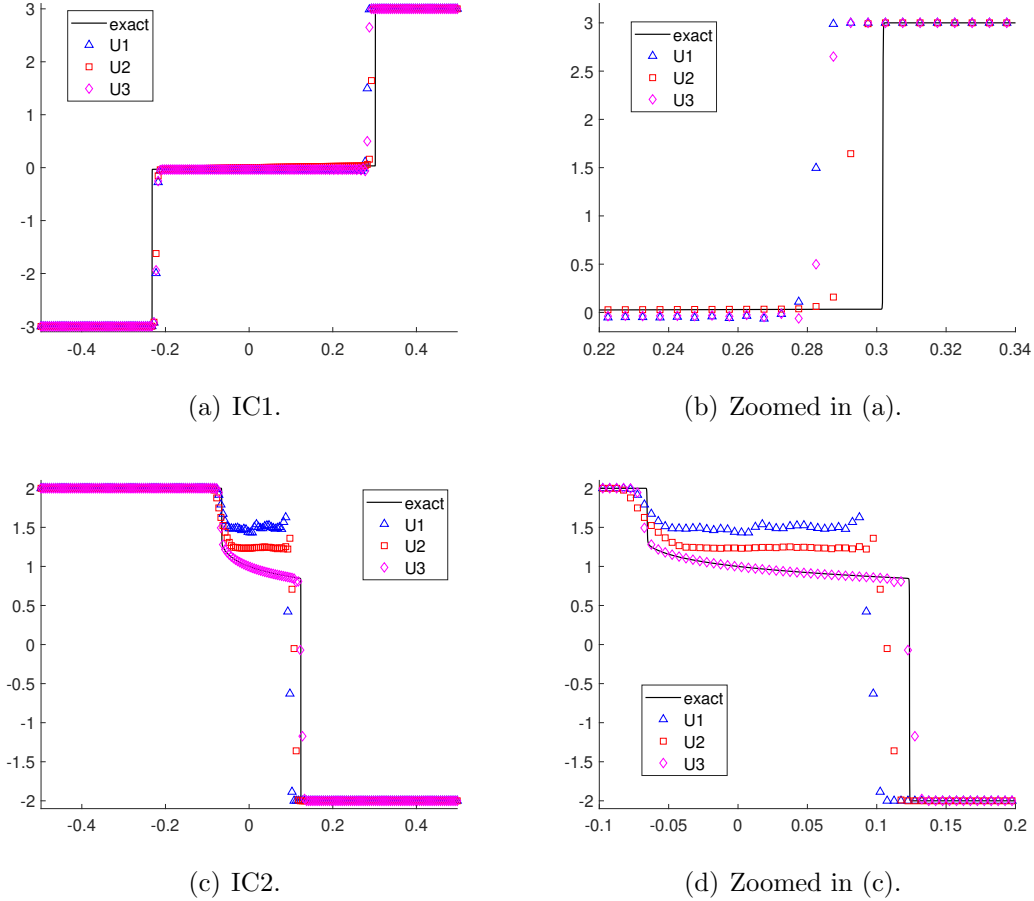


Figure 4.4. Example 4.3: One dimensional Buckley-Leverett problem with different initial conditions. Numerical solutions at $T = 1$ with $N = 200$ cells.

4.2 Two-dimensional tests

Example 4.4. (*Burgers' equation.*)

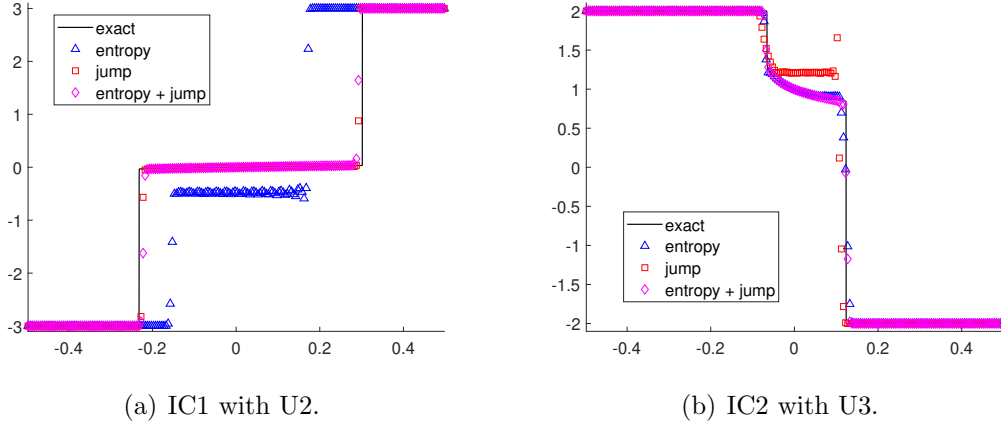


Figure 4.5. Example 4.3: One dimensional Buckley-Leverett problem with different settings of σ . Numerical solutions at $T = 1$ with $N = 200$ cells.

Here we consider the two-dimensional Burgers' equation

$$u_t + \left(\frac{u^2}{2} \right)_x + \left(\frac{u^2}{2} \right)_y = 0.$$

The computational domain is $\Omega = [0, 2\pi] \times [0, 2\pi]$ with periodic boundary conditions in each direction. The initial condition is given as

$$u(x, y, 0) = \sin(x + y).$$

In this example, we choose the entropy function as $U(u) = \cosh(u)$.

At first, we perform accuracy test at the final time $T = 0.3$, when the solution is still smooth. Errors and orders are presented in Table 4.3. We can clearly observe that the scheme achieves the designed $(k + 1)$ -th order accuracy. Next, in Figure 4.6, we plot the numerical solution with $N_x = N_y = 200$ at final time $T = 0.8$, when shocks have already appeared. A one-dimensional cut at $x = y$ of the solution is also presented. We can see that the shocks are well resolved without spurious oscillations. In Figure 4.8(a), we present the evolution of total entropy with time. It can be seen that the entropy does not increasing.

Example 4.5. (*KPP problem.*)

In this example, we consider the two-dimensional KPP problem [25]

$$u_t + (\sin u)_x + (\cos u)_y = 0,$$

which is very challenging for many high-order numerical schemes because the solution has a two-dimensional composite wave structure. The computational domain is taken as

Table 4.3. Example 4.4: Two-dimensional Burgers' equation. Errors and orders at final time $T = 0.3$.

	$N_x \times N_y$	L^1 error	order	L^2 error	order	L^∞ error	order
$k = 1$	64×64	1.85E-03	—	4.95E-03	—	4.78E-02	—
	128×128	2.47E-04	2.91	5.12E-04	3.27	4.86E-03	3.30
	256×256	5.07E-05	2.28	1.04E-04	2.30	7.49E-04	2.70
	512×512	1.27E-05	1.99	2.63E-05	1.99	1.90E-04	1.98
$k = 2$	64×64	4.73E-05	—	1.08E-04	—	1.04E-03	—
	128×128	5.83E-06	2.91	1.47E-05	2.88	1.23E-04	3.08
	256×256	7.59E-07	2.94	2.00E-06	2.88	2.06E-05	2.59
	512×512	9.78E-08	2.96	2.69E-07	2.90	3.12E-06	2.72
$k = 3$	64×64	3.64E-06	—	1.25E-05	—	1.50E-04	—
	128×128	2.13E-07	4.09	7.59E-07	4.04	1.07E-05	3.82
	256×256	1.35E-08	3.98	4.67E-08	4.02	5.49E-07	4.28
	512×512	8.53E-10	3.98	2.96E-09	3.98	3.48E-08	3.98

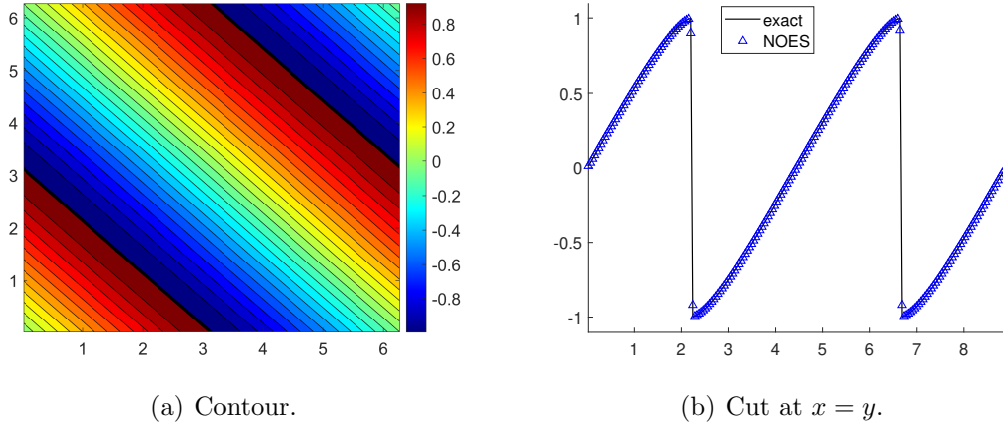


Figure 4.6. Example 4.4: Two-dimensional Burgers' equation. The numerical solution at $T = 0.8$ with $N_x = N_y = 200$.

$\Omega = [-1.5, 1.5] \times [-2, 1]$ with periodic boundary condition in each direction. The initial data is given as

$$u(x, y, 0) = \begin{cases} 3.5\pi, & x^2 + y^2 < 0.5, \\ 0.25\pi, & \text{otherwise.} \end{cases}$$

In this example, we take the entropy function as $U = \cosh(u)$. In Figure 4.7, we present the result at $T = 1$ with 200×200 meshes. It can be seen that our result agrees well with that in [25]. In Figure 4.8(b), we present the evolution with total entropy, and it is not increasing with time.

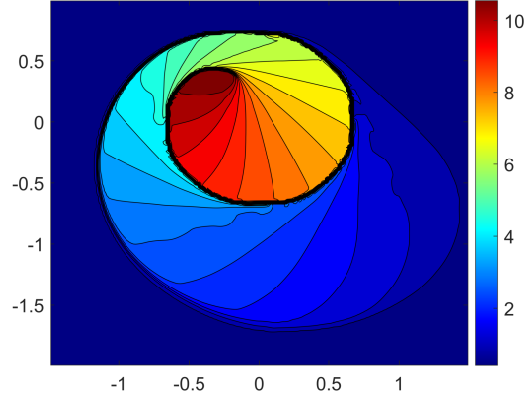


Figure 4.7. Example 4.5: KPP problem. The numerical solution at $T = 1$ with $N_x \times N_y = 200 \times 200$.

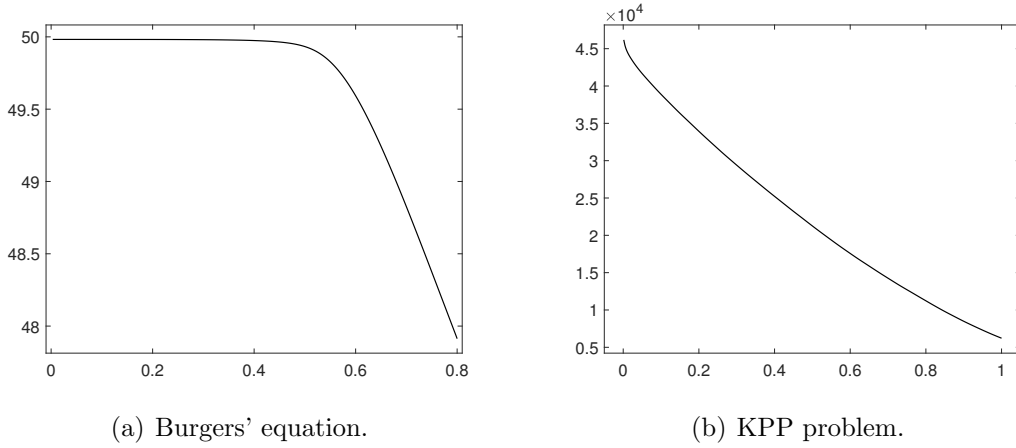


Figure 4.8. Two-dimensional tests: The evolution of total entropy with time.

4.3 Euler system

For Euler system, we employ the HLL flux in the simulations. The PP limiter is utilized on each stage of the RK method used.

Example 4.6. (1D accuracy test.)

At first, we test the accuracy of the scheme on one-dimensional Euler equation. The computational domain is $\Omega = [0, 2\pi]$ with periodic boundary condition, the initial data is given by

$$(\rho, u, p)|_{t=0} = (1 + 0.2 \sin x, 1, 1).$$

The exact solution is

$$(\rho, u, p) = (1 + 0.2 \sin(x - t), 1, 1).$$

In Table 4.4, we present the errors and orders of ρ at $T = 1$. Clearly, the optimal convergence rate is obtained.

Table 4.4. Example 4.6: One-dimensional Euler equation. Errors and orders of density ρ with the final time $T = 1$.

	N	L^1 error	order	L^2 error	order	L^∞ error	order
$k = 1$	64	6.33e-05	–	8.29e-05	–	2.59e-04	–
	128	1.58e-05	2.01	2.07e-05	2.00	6.53e-05	1.99
	256	3.94e-06	2.00	5.18e-06	2.00	1.64e-05	1.99
	512	9.83e-07	2.00	1.30e-06	2.00	4.11e-06	2.00
$k = 2$	64	5.23e-07	–	6.70e-07	–	2.75e-06	–
	128	6.48e-08	3.01	8.19e-08	3.03	2.60e-07	3.40
	256	8.09e-09	3.00	1.02e-08	3.00	3.06e-08	3.09
	512	1.01e-09	3.00	1.28e-09	3.00	3.80e-09	3.01
$k = 3$	64	3.15e-09	–	4.06e-09	–	1.21e-08	–
	128	1.93e-10	4.03	2.48e-10	4.03	6.01e-10	4.33
	256	1.20e-11	4.00	1.55e-11	4.00	3.48e-11	4.11
	512	7.57e-13	3.99	9.71e-13	3.99	2.27e-12	3.94

Example 4.7. (Sod shock tube.)

Here, we test the 1D Sod shock tube problem [34], which is a standard example for Euler equation. The computational domain is taken as $\Omega = [0, 1]$, and the initial data is given by

$$(\rho, u, p) = \begin{cases} (1, 0, 1), & x < 0.5, \\ (0.125, 0, 0.1), & x \geq 0.5. \end{cases}$$

In Figure 4.9, we compare the result of density at $T = 0.2$ with exact solution on $N = 200$ meshes. We can see the results are well-resolved and nonoscillatory.

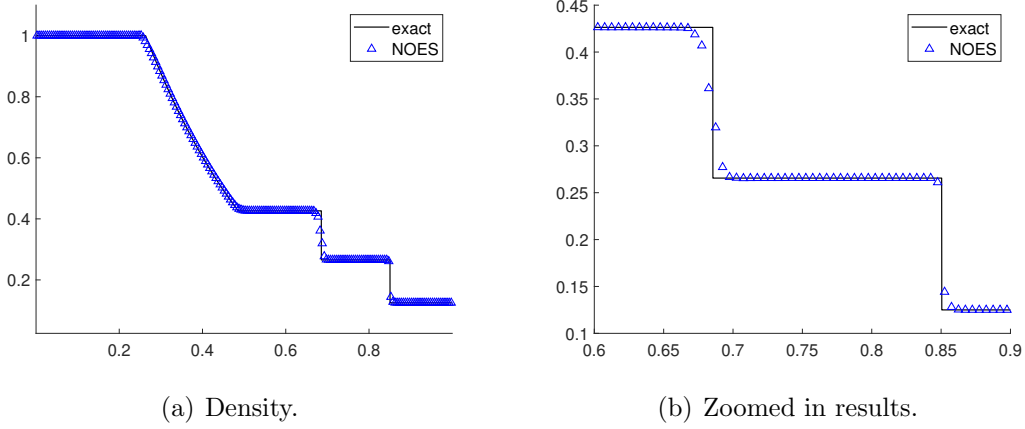


Figure 4.9. Example 4.7: Sod shock tube. The numerical solution at $T = 0.2$ with $N = 200$.

Example 4.8. (*Shu-Osher problem.*)

Next, we test the Shu-Osher problem [33]. The solution has complicated structure in that it contains both strong and weak shock waves and highly oscillatory smooth waves. The computational domain is taken as $\Omega = [-5, 5]$. And the initial data is

$$(\rho, u, p) = \begin{cases} (3.857143, 2.629369, 10.3333), & x < -4, \\ (1 + 0.2 \sin(5x), 0, 1), & x \geq 4. \end{cases}$$

In Figure 4.10, we present the results of density and pressure at $T = 1.8$ with $N = 200$. The reference solution is computed by the fifth-order finite difference WENO scheme with 2000 cells. Our numerical results seem to agree with the reference solution very well.

Example 4.9. (*Two blast waves.*)

Here, we consider the two blast-waves problem [40], which is very challenging to most of the high-order schemes. The computational domain is $\Omega = [0, 1]$ with reflective boundary conditions imposed on both end points, and the initial data is given by

$$\rho = 1, \quad u = 0, \quad p = \begin{cases} 1000, & x < 0.1, \\ 0.01, & 0.1 \leq x \leq 0.9, \\ 100, & x > 0.9. \end{cases}$$

In Figure 4.11, we present the result of density at $T = 0.038$ with $N = 800$ cells. The reference solution is obtained with the fifth-order WENO scheme with 2000 cells. Notice

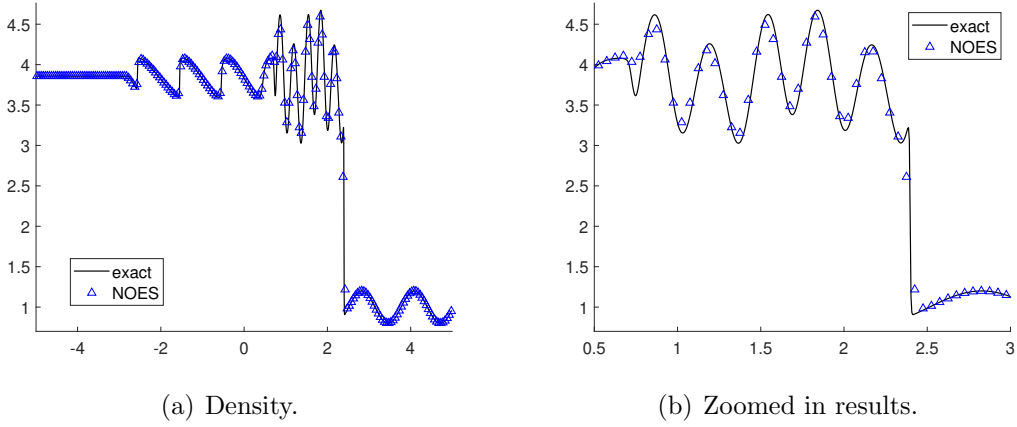


Figure 4.10. Example 4.8: Shu-Osher problem. The density of numerical solution at $T = 1.8$ with $N = 200$.

that the classical DG scheme suffers from negative pressure or negative density in this examples. However, our proposed scheme with PP limiter performs well.

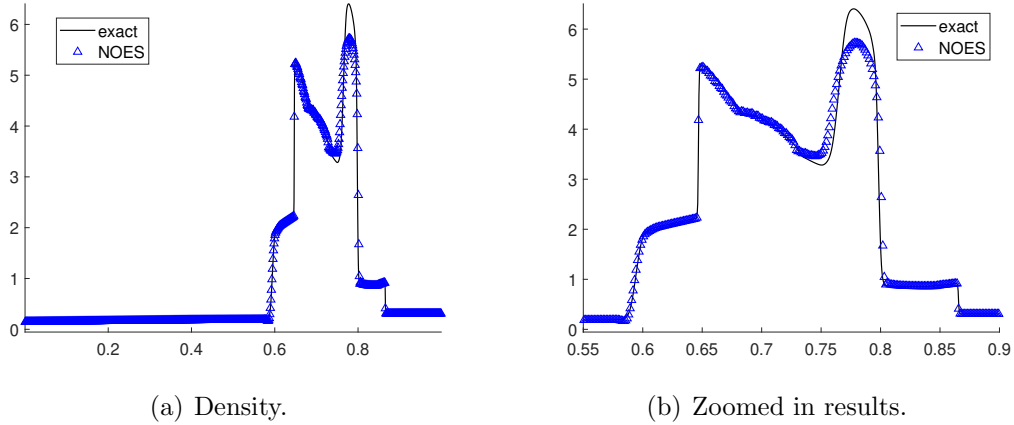


Figure 4.11. Example 4.9: Two blast waves. The density of numerical solution at $T = 0.038$ with $N_x = 800$.

Example 4.10. (*Leblanc shock tube.*)

Here, we consider the Leblanc problem [31], which is an extremely Riemann problem with very strong discontinuities and is used to test robustness of our scheme. The computational domain is $\Omega = [-10, 10]$, and the initial data is given by

$$(\rho, u, p) = \begin{cases} (2, 0, 10^9), & x < 0, \\ (0.001, 0, 1), & x \geq 0. \end{cases}$$

In Figure 4.12, we compare the result of density, velocity and pressure with the exact solution at $T = 0.0001$ on $N = 800$ and $N = 6400$ meshes. These results show the robustness and convergence of our scheme.

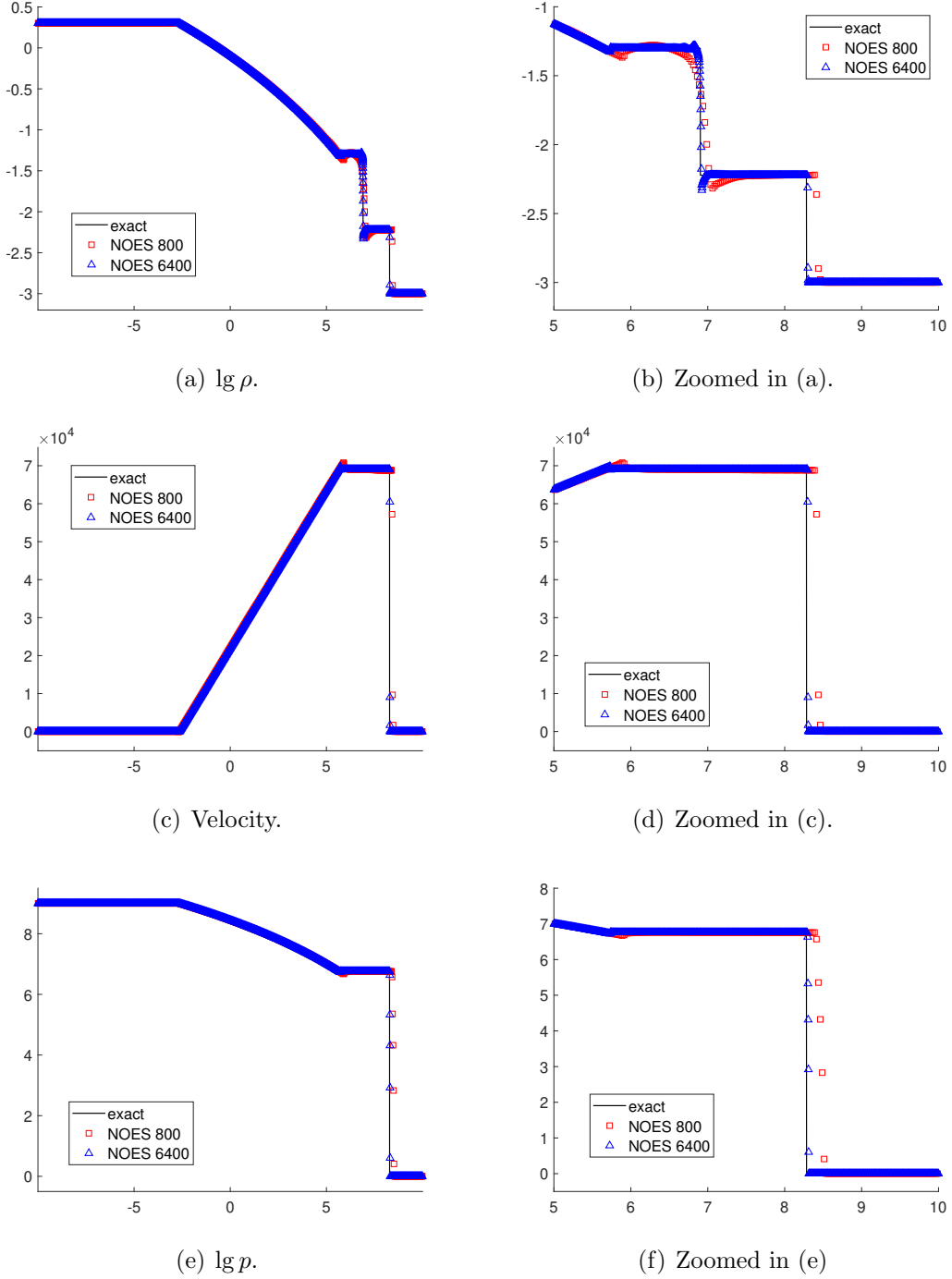


Figure 4.12. Example 4.10: Leblanc shock tube. The numerical solution at $T = 0.0001$ with $N = 800$ and $N = 6400$.

Example 4.11. (2D accuracy test.)

We test the accuracy of the scheme for two-dimensional Euler equation. Initially, an isentropic vortex perturbation centered at $(5, 0)$ is added on the mean flow $(\rho_0, u_0, v_0, p_0) = (1, 1, 0, 1)$:

$$\begin{aligned}\rho &= \left(1 - \frac{\gamma - 1}{16\gamma\pi^2}\beta^2 e^{2(1-r^2)}\right)^{1/(\gamma-1)}, \\ u &= 1 - \frac{\beta}{2\pi}ye^{1-r^2}, \\ v &= \frac{\beta}{2\pi}(x - 5)e^{1-r^2}, \\ p &= \rho^\gamma,\end{aligned}$$

where $r^2 = (x - 5)^2 + y^2$ and we take the vortex strength $\beta = 5$. This problem is essential nonlinear. It is clear that the exact solution is just the passive convection of the vortex with the mean velocity. In numerical simulation, we take the computational domain is $\Omega = [0, 10] \times [-5, 5]$ extended periodically in both directions. In Table 4.5, we present the errors and orders of accuracy of ρ at $T = 10$. At this time, the exact solution will coincide with the initial data. It can be seen that the optimal convergence rate is obtained.

Table 4.5. Example 4.4: Two-dimensional isentropic vortex problem. Errors and orders of density with the final time $T = 10$.

	$N_x \times N_y$	L^1 error	order	L^2 error	order	L^∞ error	order
$k = 1$	64×64	6.43e-04	–	2.15e-03	–	2.08e-02	–
	128×128	9.89e-05	2.70	3.35e-04	2.68	3.58e-03	2.54
	256×256	1.45e-05	2.77	4.91e-05	2.77	5.83e-04	2.62
	512×512	2.53e-06	2.52	8.29e-06	2.57	1.01e-04	2.53
	1024×1024	5.35e-07	2.24	1.73e-06	2.26	1.94e-05	2.37
$k = 2$	64×64	1.08e-05	–	3.36e-05	–	5.36e-04	–
	128×128	1.01e-06	3.42	2.96e-06	3.50	5.88e-05	3.19
	256×256	1.26e-07	3.00	3.75e-07	2.98	7.08e-06	3.06
	512×512	1.65e-08	2.93	5.14e-08	2.87	8.77e-07	3.01
$k = 3$	64×64	6.17e-07	–	1.83e-06	–	3.45e-05	–
	128×128	2.61e-08	4.57	8.63e-08	4.41	1.72e-06	4.33
	256×256	1.38e-09	4.24	4.89e-09	4.14	1.10e-07	3.97
	512×512	8.90e-11	3.96	3.07e-10	3.99	6.70e-09	4.04

Example 4.12. (2D Riemann problem.)

Two-dimensional Riemann problems with different initial configurations have been extensively employed to examine the numerical schemes for Euler equations. Here, We

consider the case in [26]. The computational domain is $\Omega = [0, 1] \times [0, 1]$ with outflow boundary conditions. The initial data is given by

$$(\rho, u, v, p) = \begin{cases} (1.5, 0, 0, 1.5), & (x, y) \in (0.8, 1] \times (0.8, 1], \\ (0.5323, 1.206, 0, 0.3), & (x, y) \in [0, 0.8) \times (0.8, 1], \\ (0.138, 1.206, 1.206, 0.029), & (x, y) \in [0, 0.8) \times [0, 0.8), \\ (0.5323, 0, 1.206, 0.3), & (x, y) \in (0.8, 1] \times [0, 0.8). \end{cases}$$

In Figure 4.13, we present the result of density at $T = 0.8$ with $N_x = N_y = 400$. It can be seen that the reflection shocks and contact discontinuities are captured well.

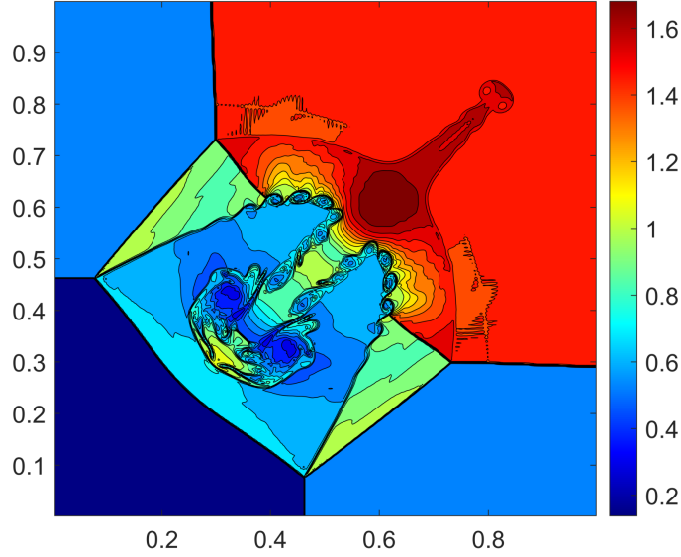


Figure 4.13. Example 4.12: Two-dimensional Riemann problem. The numerical solution of density at $T = 0.8$ with $N_x = N_y = 400$. 30 contour lines are used.

Example 4.13. (*Double Mach reflection.*)

Next, we consider the double-Mach reflection problem [40], which is a benchmark test problem for the two-dimensional Euler equation. The computational domain is $\Omega = [0, 4] \times [0, 1]$. The reflection wall lies at the bottom of the computational domain starting from $x = 1/6$. This problem describes a right-moving Mach 10 shock initially positioned at $x = 1/6, y = 0$, makes a 60° angle with the horizontal wall, i.e.,

$$(\rho, u, v, p) = \begin{cases} (8, 8.25 \cos(\frac{\pi}{6}), 8.25 \sin(\frac{\pi}{6}), 116.5), & x < \frac{1}{6} + \frac{y}{\sqrt{3}}, \\ (1.4, 0, 0, 1), & x \geq \frac{1}{6} + \frac{y}{\sqrt{3}}. \end{cases}$$

The inflow and outflow conditions are imposed on the left and the right boundary respectively. For the bottom boundary, the exact post-shock boundary condition is imposed for the part $0 < x < 1/6$, and a reflective boundary is used for the rest. For the top boundary, the post-shock condition is imposed for the part from $0 < x < 1/6 + (1 + 20t)/\sqrt{3}$, and the pre-shock condition is used for the rest. In Figure 4.14, we present the result at $T = 0.2$ with $N_x \times N_y = 960 \times 240$ and $N_x \times N_y = 1920 \times 480$. And a zoomed-in graph is provided in Figure 4.15. We can see that our results agree well with the results in [40].

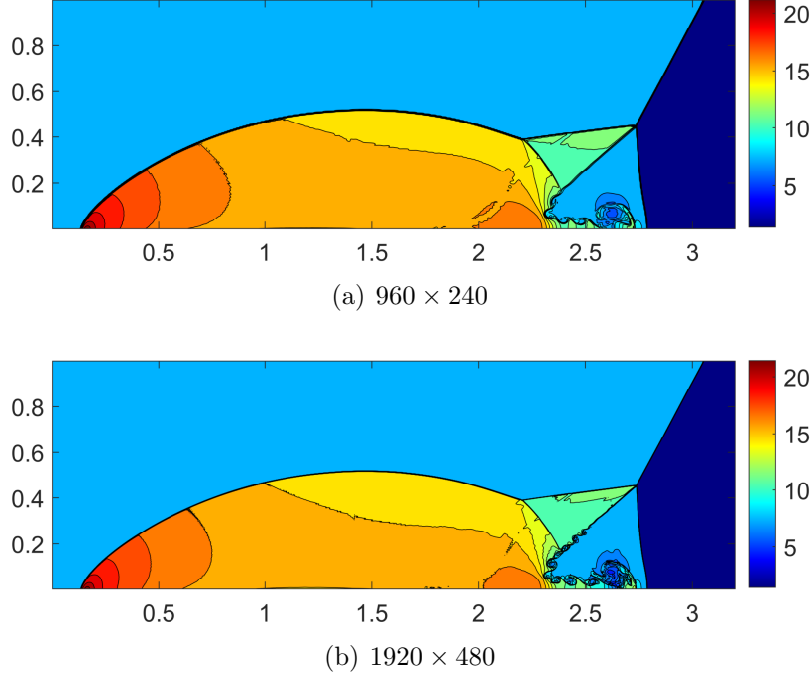


Figure 4.14. Example 4.13: Double Mach reflection. The numerical solution of density at $T = 0.2$. 30 contour lines are used.

Example 4.14. (*Mach 2000 jet.*)

Finally, we consider the high Mach number astrophysical jet problem [41]. We note that $\gamma = 5/3$ in this example. In this example, the code could easily produce the negative pressure and density, resulting in blow up easily during numerical computation.

The computational domain is $\Omega = [0, 1] \times [-0.25, 0.25]$, initially full of the ambient gas with

$$(\rho, u, v, p) = (0.5, 0, 0, 0.4127).$$

A Mach 2000 jet state $(\rho, u, v, p) = (5, 800, 0, 0.4127)$ is injected from the left boundary in the range $-0.05 < y < 0.05$. Outflow conditions are applied on all remaining boundaries.

In Figure 4.16, we present the density, pressure and temperature p/ρ at time $T = 0.001$ with 320×160 meshes. It is observed that our scheme can capture the feature without any occurrence of instability, indicating the efficiency of our proposed schemes.

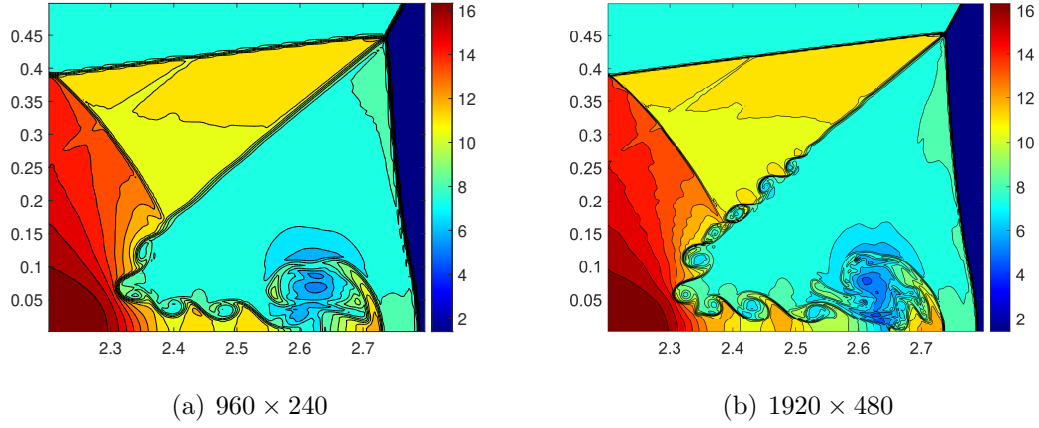


Figure 4.15. Example 4.13: Double Mach reflection. Zoomed-in figure. The numerical solution of density near the Mach stem at $T = 0.2$. 30 contour lines are used.

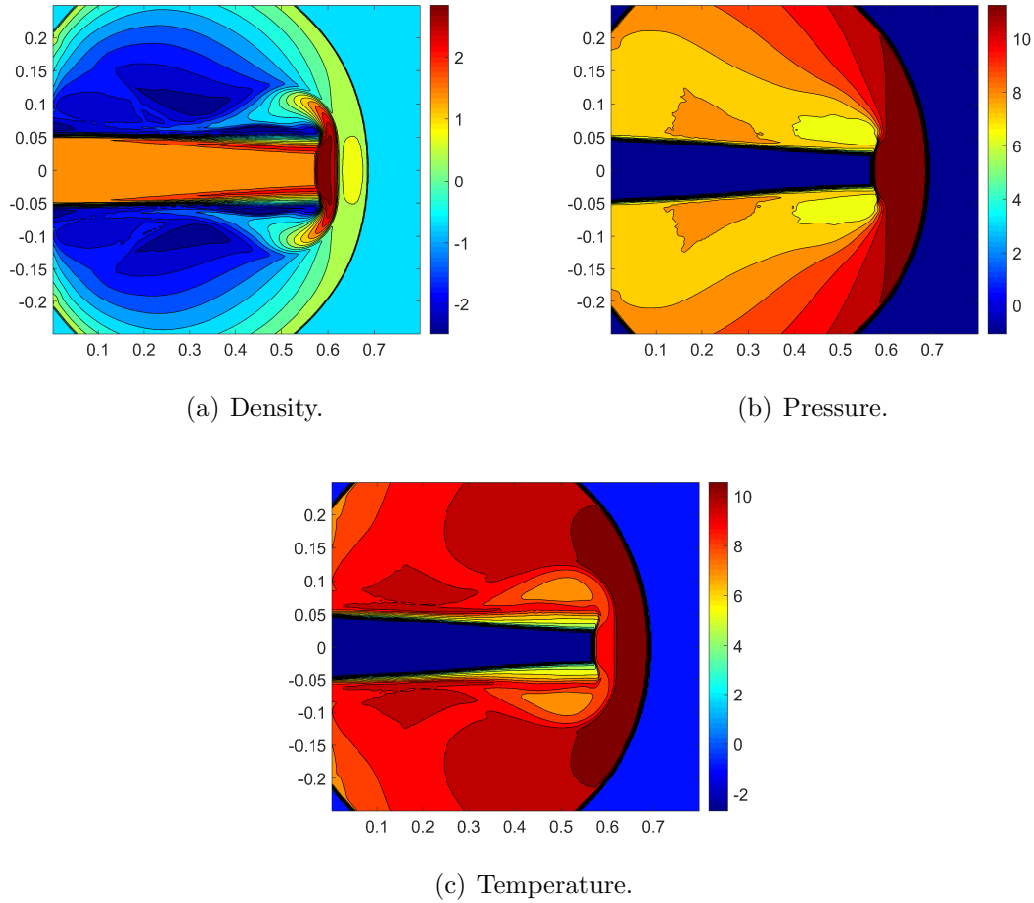


Figure 4.16. Example 4.14: High Mach number jet problem. The numerical solution at $T = 0.001$ with $N_x \times N_y = 320 \times 160$. Scales are logarithmic. 12 contour lines are used.

5 Concluding remarks

In this paper, we present a class of non-oscillatory entropy-stable DG methods for solving hyperbolic conservation laws. By incorporating a specific form of local artificial viscosity term into the original DG scheme on each cell and imposing an interpolation condition, the semi-discrete scheme ensures strict non-increase of the total entropy with a careful design of the viscosity coefficient. An oscillation coefficient is taken into account to control spurious oscillation near shock waves. Moreover, the oscillation coefficient is also used to limit viscosity parameter for cases where the denominator of the entropy coefficient approaches zero. We prove the optimal accuracy for scalar advection equations with quadratic entropy, and advection equations with other entropy functions under certain assumptions. It is noted that large viscosity terms can induce stiffness and impose strict constraints on time step sizes. To address this, we employ the integration factor Runge-Kutta method, enabling explicit computation under standard CFL conditions. Due to the local structure of our proposed scheme, the algorithm can be implemented easily. For extreme problems where negative pressures might occur, we prove that our scheme is compatible with positivity-preserving limiters under suitable CFL conditions. Extensive numerical examples confirm that our scheme guarantees entropy decrease, controls oscillations, and achieves optimal accuracy. Future work may include extending this method to unstructured meshes and applying it to other equations.

Acknowledgements

The authors would like to express their gratitude to Professor Yang Yang for his valuable discussions.

References

- [1] R. Abgrall. A general framework to construct schemes satisfying additional conservation relations. Application to entropy conservative and entropy dissipative schemes. *Journal of Computational Physics*, 2018.
- [2] M. Carpenter, T. Fisher, E. Nielsen, M. Parsani, M. Svård, and N. Yamaleev. Entropy stable summation-by-parts formulations for compressible computational fluid dynamics. In *Handbook of Numerical Analysis*, volume 17, pages 495–524. Elsevier, 2016.
- [3] M. H. Carpenter, T. C. Fisher, E. J. Nielsen, and S. H. Frankel. Entropy stable spectral collocation schemes for the Navier–Stokes equations: Discontinuous interfaces. *SIAM Journal on Scientific Computing*, 36(5):B835–B867, 2014.

- [4] J. Chan. On discretely entropy conservative and entropy stable discontinuous Galerkin methods. *Journal of Computational Physics*, 362:346–374, 2018.
- [5] J. Chan, D. C. Del Rey Fernández, and M. H. Carpenter. Efficient entropy stable Gauss collocation methods. *SIAM Journal on Scientific Computing*, 41(5):A2938–A2966, 2019.
- [6] S. Chen. Krylov SSP Integrating Factor Runge–Kutta WENO Methods. *Mathematics*, 9(13):1483, 2021.
- [7] T. Chen and C.-W. Shu. Entropy stable high order discontinuous Galerkin methods with suitable quadrature rules for hyperbolic conservation laws. *Journal of Computational Physics*, 345:427–461, 2017.
- [8] T. Chen and C.-W. Shu. Review of entropy stable discontinuous Galerkin methods for systems of conservation laws on unstructured simplex meshes. *CSIAM Transactions on Applied Mathematics*, 1(1):1–52, 2020.
- [9] B. Cockburn, G. Kanschat, I. Perugia, and D. Schötzau. Superconvergence of the local discontinuous Galerkin method for elliptic problems on Cartesian grids. *SIAM Journal on Numerical Analysis*, 39(1):264–285, 2001.
- [10] D. C. Del Rey Fernández, J. E. Hicken, and D. W. Zingg. Simultaneous approximation terms for multi-dimensional summation-by-parts operators. *Journal of Scientific Computing*, 75:83–110, 2018.
- [11] D. C. D. R. Fernández, P. D. Boom, and D. W. Zingg. A generalized framework for nodal first derivative summation-by-parts operators. *Journal of Computational Physics*, 266:214–239, 2014.
- [12] D. C. D. R. Fernández, J. E. Hicken, and D. W. Zingg. Review of summation-by-parts operators with simultaneous approximation terms for the numerical solution of partial differential equations. *Computers & Fluids*, 95:171–196, 2014.
- [13] T. C. Fisher and M. H. Carpenter. High-order entropy stable finite difference schemes for nonlinear conservation laws: Finite domains. *Journal of Computational Physics*, 252:518–557, 2013.
- [14] U. S. Fjordholm, S. Mishra, and E. Tadmor. Arbitrarily high-order accurate entropy stable essentially nonoscillatory schemes for systems of conservation laws. *SIAM Journal on Numerical Analysis*, 50(2):544–573, 2012.
- [15] E. Gaburro, P. Öffner, M. Ricchiuto, and D. Torlo. High order entropy preserving ADER-DG schemes. *Applied Mathematics and Computation*, 440:127644, 2023.

- [16] G. J. Gassner. A skew-symmetric discontinuous Galerkin spectral element discretization and its relation to SBP-SAT finite difference methods. *SIAM Journal on Scientific Computing*, 35(3):A1233–A1253, 2013.
- [17] G. J. Gassner, A. R. Winters, and D. A. Kopriva. A well balanced and entropy conservative discontinuous Galerkin spectral element method for the shallow water equations. *Applied Mathematics and Computation*, 272:291–308, 2016.
- [18] J.-L. Guermond, R. Pasquetti, and B. Popov. Entropy viscosity method for nonlinear conservation laws. *Journal of Computational Physics*, 230(11):4248–4267, 2011.
- [19] A. Harten. On the symmetric form of systems of conservation laws with entropy. *Journal of Computational Physics*, 49(1):151–164, 1983.
- [20] J. S. Hesthaven. From electrostatics to almost optimal nodal sets for polynomial interpolation in a simplex. *SIAM Journal on Numerical Analysis*, 35(2):655–676, 1998.
- [21] J. E. Hicken, D. C. Del Rey Fernández, and D. W. Zingg. Multidimensional summation-by-parts operators: general theory and application to simplex elements. *SIAM Journal on Scientific Computing*, 38(4):A1935–A1958, 2016.
- [22] T. Hughes, L. Franca, and M. Mallet. A new finite element formulation for computational fluid dynamics: I. Symmetric forms of the compressible Euler and Navier-Stokes equations and the second law of thermodynamics. *Computer Methods in Applied Mechanics and Engineering*, 54(2):223–234, 1986.
- [23] G. S. Jiang and C.-W. Shu. On a cell entropy inequality for discontinuous Galerkin methods. *Mathematics of Computation*, 62(206):531–538, 1994.
- [24] D. I. Ketcheson. Relaxation Runge–Kutta methods: Conservation and stability for inner-product norms. *SIAM Journal on Numerical Analysis*, 57(6):2850–2870, 2019.
- [25] A. Kurganov, G. Petrova, and B. Popov. Adaptive semidiscrete central-upwind schemes for nonconvex hyperbolic conservation laws. *SIAM Journal on Scientific Computing*, 29(6):2381–2401, 2007.
- [26] A. Kurganov and E. Tadmor. Solution of two-dimensional Riemann problems for gas dynamics without Riemann problem solvers. *Numerical Methods for Partial Differential Equations: An International Journal*, 18(5):584–608, 2002.
- [27] P. Lax and B. Wendroff. Systems of conservation laws. *Communications on Pure and Applied Mathematics*, 13:217–237, 1960.

- [28] P. G. Lefloch, J.-M. Mercier, and C. Rohde. Fully discrete, entropy conservative schemes of arbitrary order. *SIAM Journal on Numerical Analysis*, 40(5):1968–1992, 2002.
- [29] R. J. LeVeque. *Finite volume methods for hyperbolic problems*, volume 31. Cambridge university press, 2002.
- [30] Y. Liu, J. Lu, and C.-W. Shu. An entropy stable essentially oscillation-free Discontinuous Galerkin method for hyperbolic conservation laws. *SIAM Journal on Scientific Computing*, 46(2):A1132–A1159, 2024.
- [31] R. Loubere and M. J. Shashkov. A subcell remapping method on staggered polygonal grids for arbitrary-Lagrangian–Eulerian methods. *Journal of Computational Physics*, 209(1):105–138, 2005.
- [32] J. Lu, Y. Liu, and C.-W. Shu. An oscillation-free Discontinuous Galerkin method for scalar hyperbolic conservation laws. *SIAM Journal on Numerical Analysis*, 59(3):1299–1324, 2021.
- [33] C.-W. Shu and S. Osher. Efficient implementation of essentially non-oscillatory shock-capturing schemes. *Journal of Computational Physics*, 77(2):439–471, 1988.
- [34] G. A. Sod. A survey of several finite difference methods for systems of nonlinear hyperbolic conservation laws. *Journal of Computational Physics*, 27(1):1–31, 1978.
- [35] M. Svärd and J. Nordström. Review of summation-by-parts schemes for initial–boundary-value problems. *Journal of Computational Physics*, 268:17–38, 2014.
- [36] E. Tadmor. The numerical viscosity of entropy stable schemes for systems of conservation laws. I. *Mathematics of Computation*, 49(179):91–103, 1987.
- [37] E. Tadmor. Entropy stability theory for difference approximations of nonlinear conservation laws and related time-dependent problems. *Acta Numerica*, 12:451–512, 2003.
- [38] E. F. Toro. The HLLC Riemann solver. *Shock waves*, 29(8):1065–1082, 2019.
- [39] L. Wei, L. Zhou, and Y. Xia. The jump filter in the discontinuous Galerkin method for hyperbolic conservation laws. *arXiv preprint arXiv:2407.19169*, 2024.
- [40] P. Woodward and P. Colella. The numerical simulation of two-dimensional fluid flow with strong shocks. *Journal of Computational Physics*, 54(1):115–173, 1984.
- [41] X. Zhang and C.-W. Shu. On positivity-preserving high order discontinuous Galerkin schemes for compressible Euler equations on rectangular meshes. *Journal of Computational Physics*, 229(23):8918–8934, 2010.

- [42] X. Zhang, Y. Xia, and C.-W. Shu. Maximum-principle-satisfying and positivity-preserving high order discontinuous Galerkin schemes for conservation laws on triangular meshes. *Journal of Scientific Computing*, 50(1):29–62, 2012.